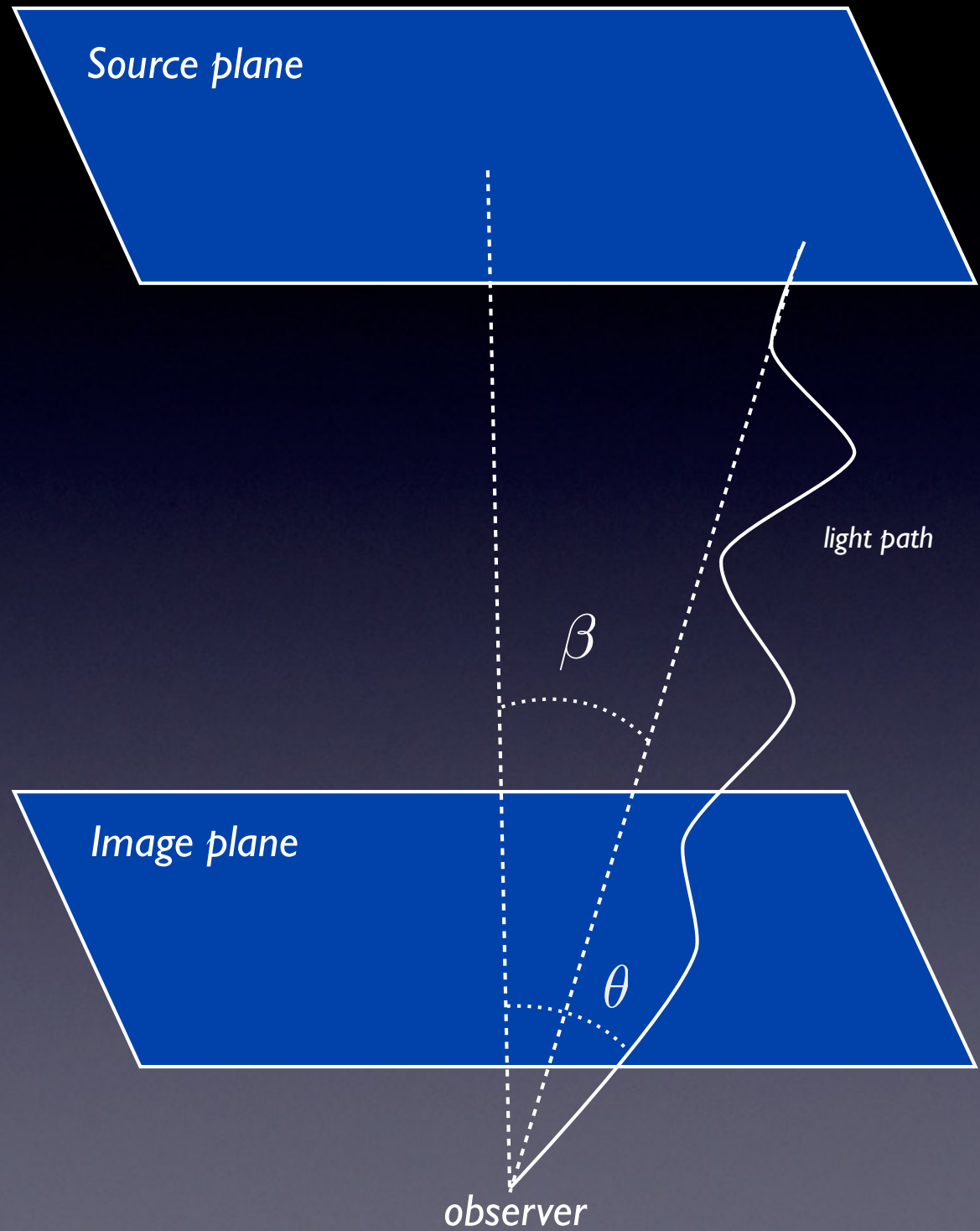# Gravitational Lensing & Cosmology

Cosmology School in the Canary Islands
R. Ben Metcalf (U. of Bologna)

- Basic concepts of Weak Lensing

- Measuring Weak Lensing from Galaxy Shear

- Lensing of the CMB

- Not covered:

  - Lensing by Galaxy Clusters
  - Strong Gravitational Lensing

ALMA MATER STUDIORUM
UNIVERSITÀ DI BOLOGNA

Source plane

Lensing Equation

$$\vec{\beta} = \vec{\theta} - \vec{\alpha}(\vec{\theta})$$

light path

β

Image plane

θ

observer

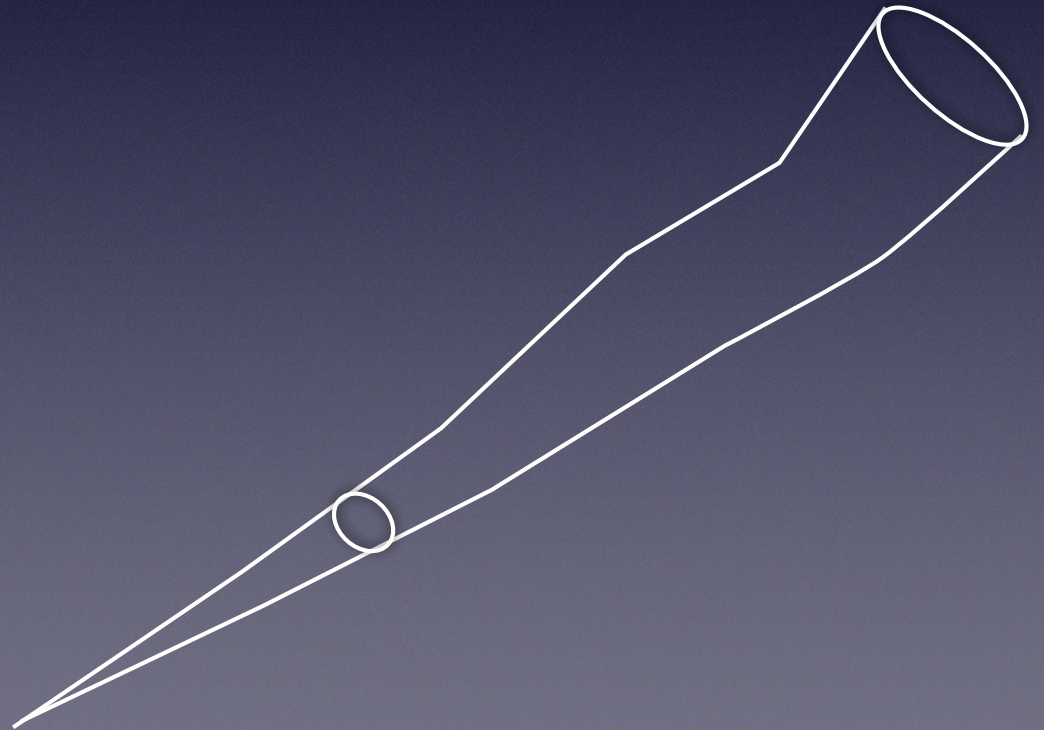$$\vec{\beta} = \vec{\theta} - \vec{\alpha}(\vec{\theta})$$

$$\frac{\partial \vec{\beta}}{\partial \vec{\theta}} = \mathbf{A} = \begin{pmatrix} 1 - \kappa - \gamma_1 & \gamma_2 \\ \gamma_2 & 1 - \kappa + \gamma_1 \end{pmatrix}$$

$$\kappa \equiv 1 - \frac{1}{2}\mathrm{tr}\mathbf{A} \quad \textit{Convergence}$$

$$\{\gamma_1, \gamma_2\} \quad \textit{Shear}$$

$$\textit{magnification}$$

$$\mu = \frac{1}{|\mathbf{A}|} = \frac{1}{(1 - \kappa)^2 - |\gamma|^2}$$

$$\gamma_1 > 0$$

$$\gamma_1 < 0$$

$$\gamma_2 > 0$$

$$\gamma_2 < 0$$

Propagation of a light ray
from geodesic equation

$$\frac{d^2 x_\perp}{d\lambda^2} = -2\nabla_\perp \Phi$$

Newtonian Potential

Source

Lens

light

β

Image

θ
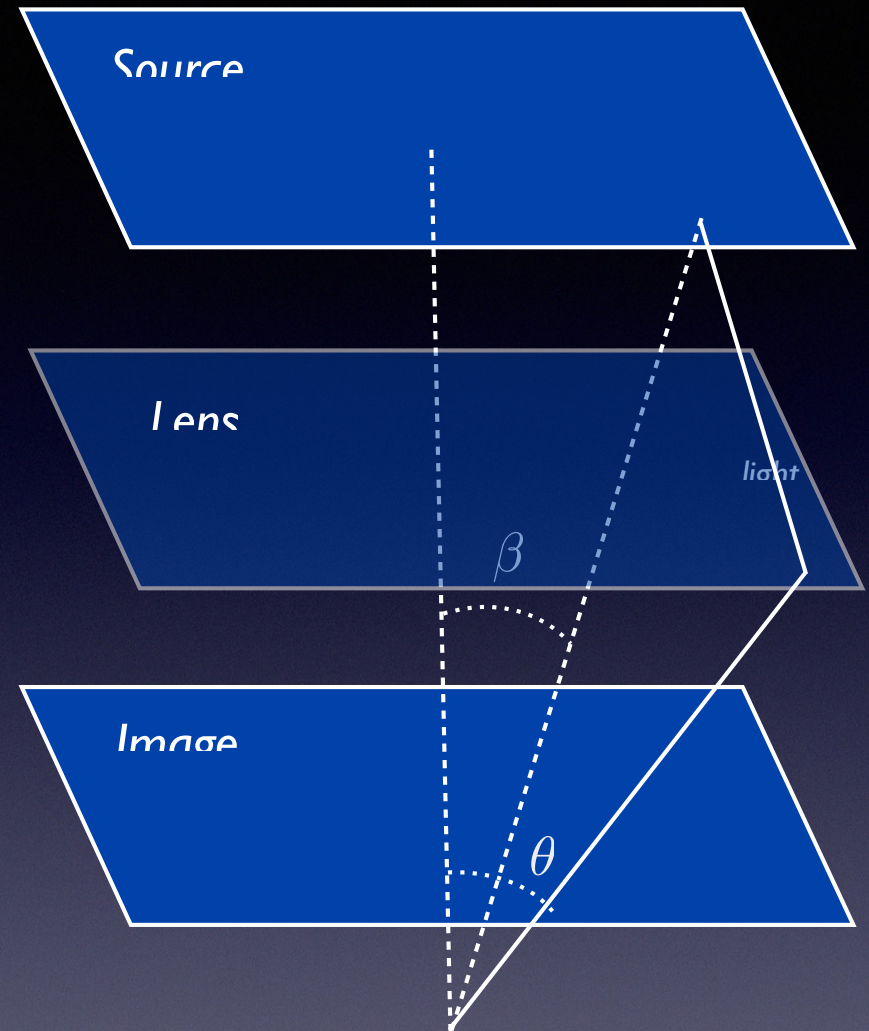
Propagation of a light ray from geodesic equation

$$\frac{d^2 x_\perp}{d\lambda^2} = -2\nabla_\perp \Phi$$

Newtonian Potential

More generally
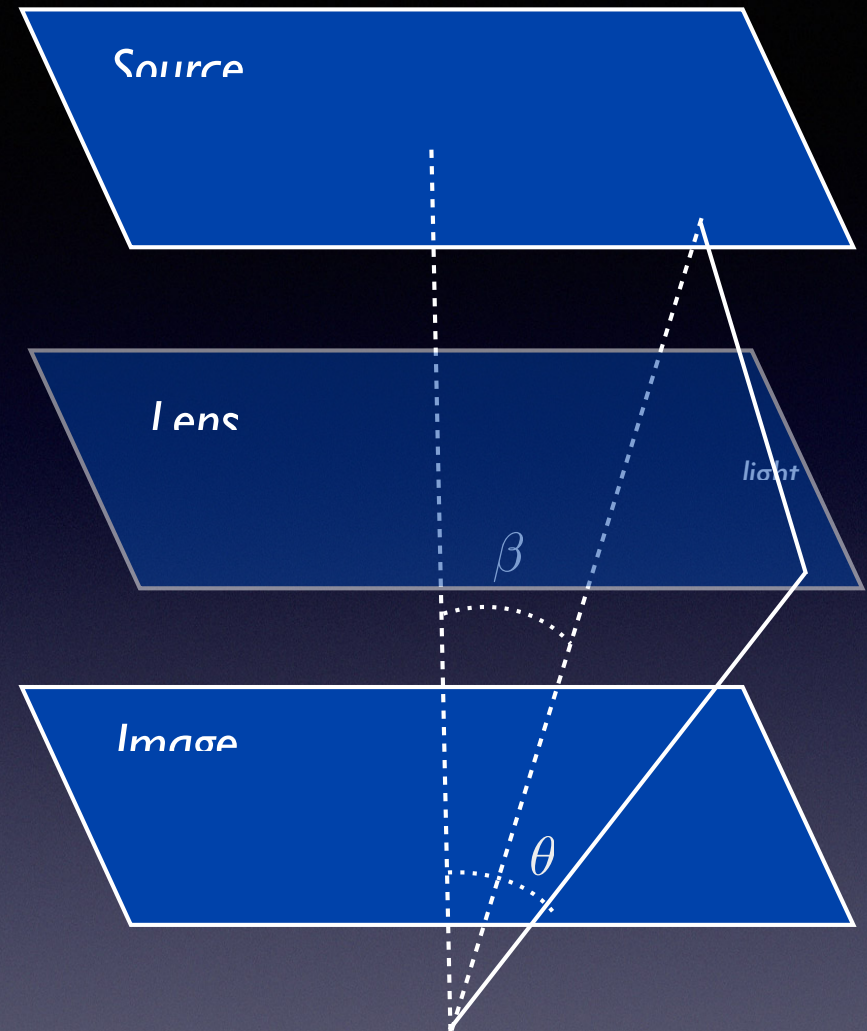
$$\frac{d^2 x_\perp}{d\lambda^2} = -\nabla_\perp(\Phi + \Psi)$$

Newtonian gauge

$\Phi = \Psi$ *Without anisotropic stress*

$$ds^2 = -(1 + 2\Psi)dt^2 + a(t)^2(1 - 2\Phi)\delta_{ij}dx^i dx^j$$

Source

Lens

light

Image

β

θ

*Propagation of a light ray
 from geodesic equation*

$$\frac{d^2 x_\perp}{d\lambda^2} = -2\nabla_\perp \Phi$$

Single Lens Plane Lens Equation

$$\vec{\beta} = \vec{\theta} - \vec{\alpha}(\vec{\theta})$$

$$\vec{\alpha} = \nabla \phi$$
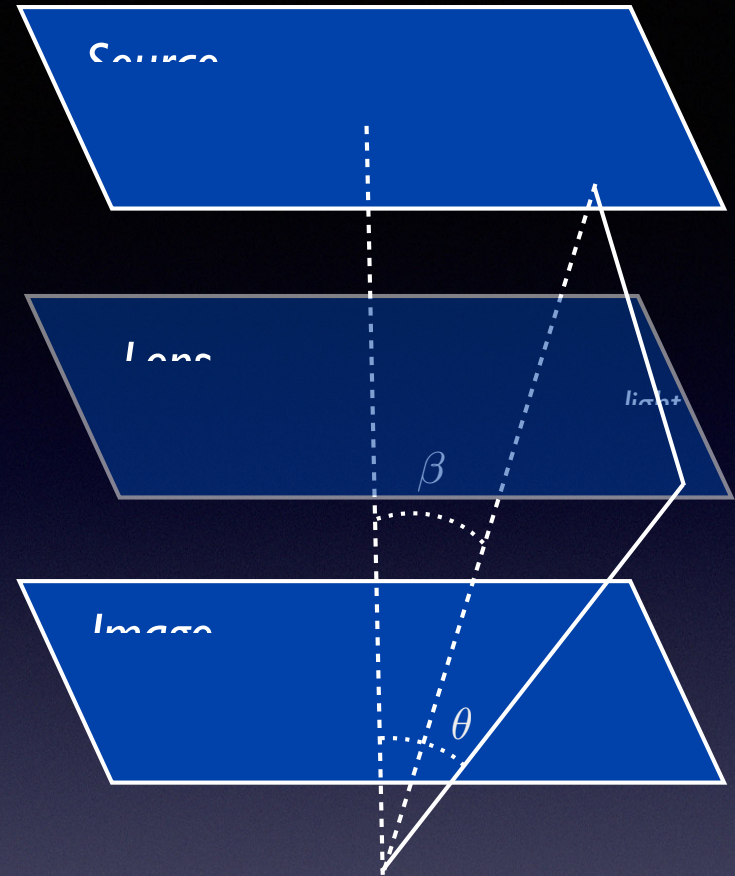
Lensing potential
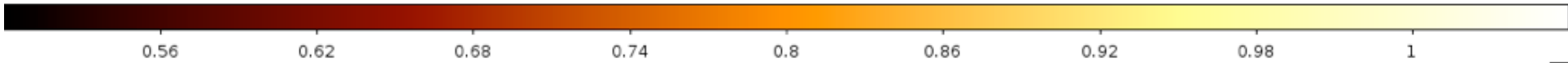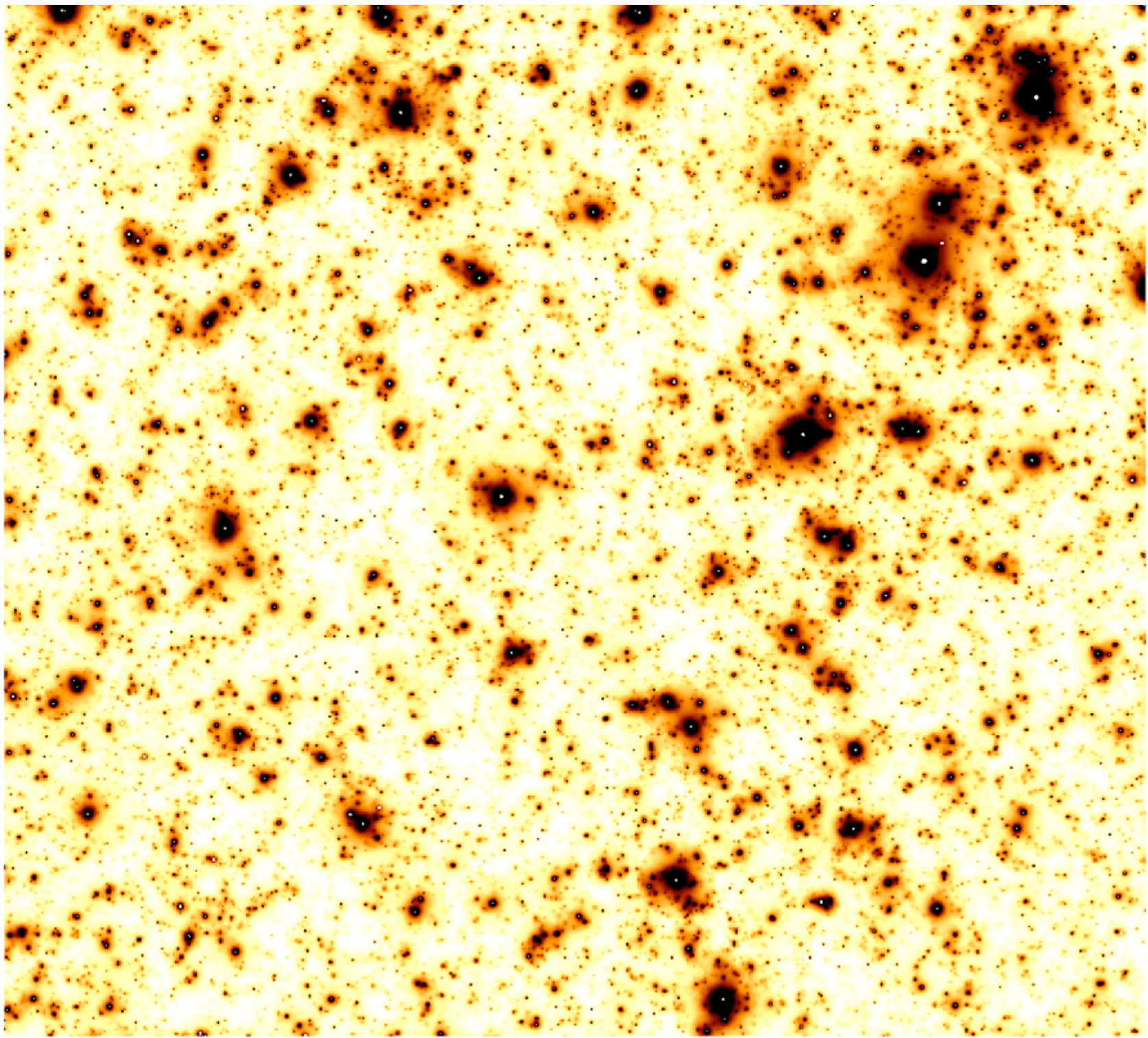
$$\nabla^2 \phi = 2\kappa$$

$$\kappa(\theta) = \frac{\Sigma(\theta)}{\Sigma_{\text{crit}}}$$

*Convergence
/ dimensionless surface density*

$$\Sigma_{\text{crit}}(z_{\text{lens}}, z_{\text{source}}) = \frac{c^2}{4\pi G} \frac{D(z_{\text{source}})}{D(z_{\text{lens}})D(z_{\text{lens}}, z_{\text{source}})}$$

Critical density

Weak Lensing in the Field

In the weak lensing limit the ellipticity of a galaxy is the intrinsic ellipticity plus the shear.

$$\vec{\epsilon} \simeq \vec{\gamma} + \vec{\epsilon}_o$$

The error in this estimator even with perfect measurements is limited by the intrinsic ellipticity of galaxies and their number density on the sky.

To measure a shear we average over the ellipticities of galaxies in a region of the sky

$$\hat{\gamma} = \frac{1}{N} \sum_i \vec{\epsilon}_i$$

$$\sigma_\gamma^2 = \langle |\hat{\gamma}|^2 \rangle - |\vec{\gamma}|^2 = \frac{1}{N^2} \sum_{ij} \langle \vec{\epsilon}_i \cdot \vec{\epsilon}_j \rangle$$

$$= \frac{1}{N^2} \sum_i \langle |\vec{\epsilon}_i|^2 \rangle$$

$$= \frac{\sigma_\epsilon^2}{N}$$

In the field $\quad \gamma \sim 0.03 \qquad \sigma_\epsilon \sim 0.3 \qquad \eta \lesssim 30 \text{ galaxies arcmin}^{-2}$

- In the field, "cosmic shear", the emphasis is on statistical measures of the shear rather than mapping of the actual mass distribution. Also cosmology generally predicts statistical properties in any case.

- Must consider deflections by multiple planes or continuous 3D potential field

- Because the signal-to-noise per galaxy is so low, errors and bias in the ellipticity, or shear estimator, becomes a critical issue.
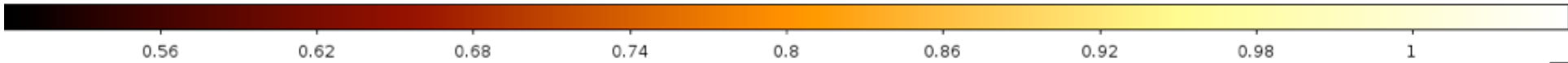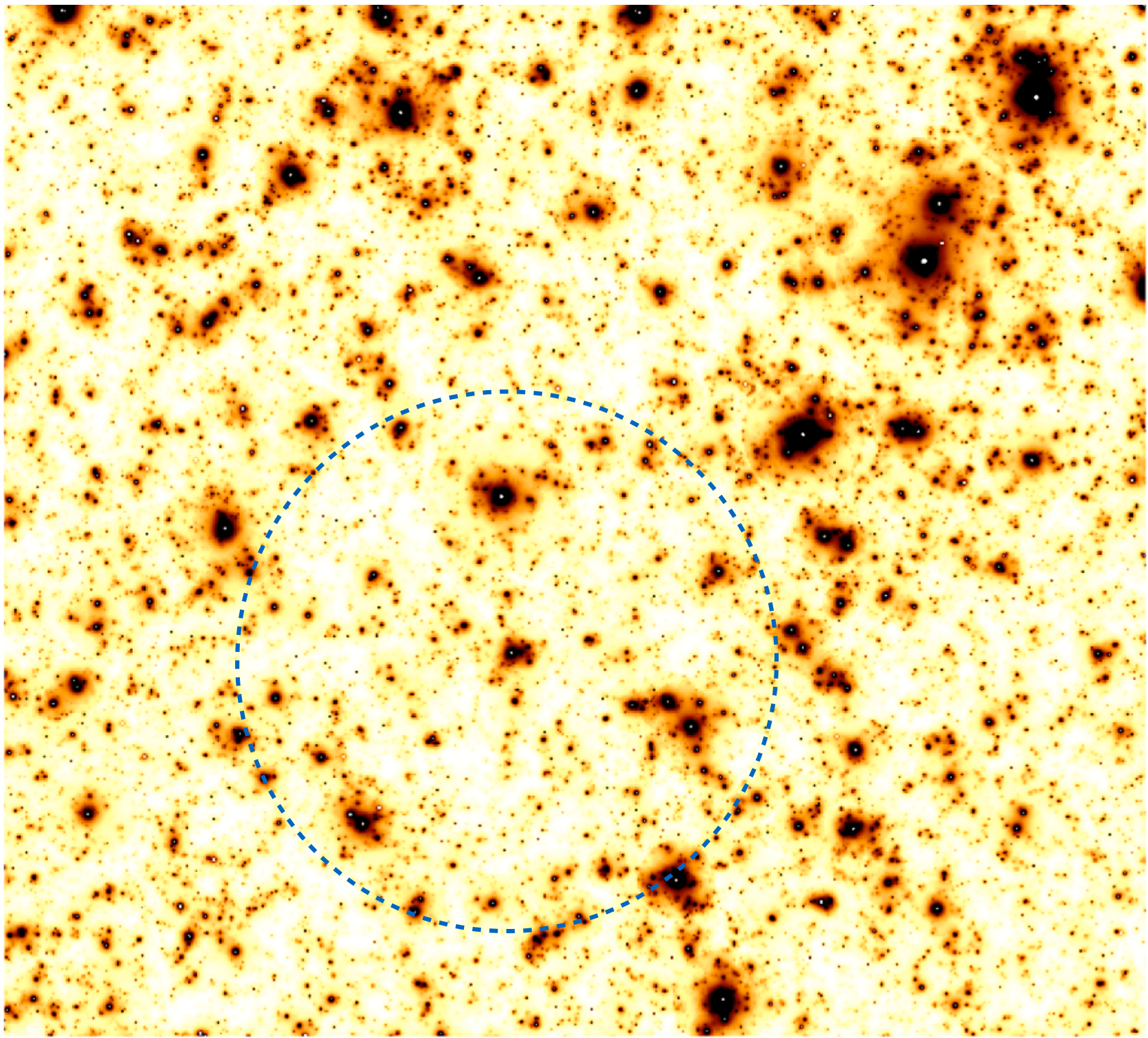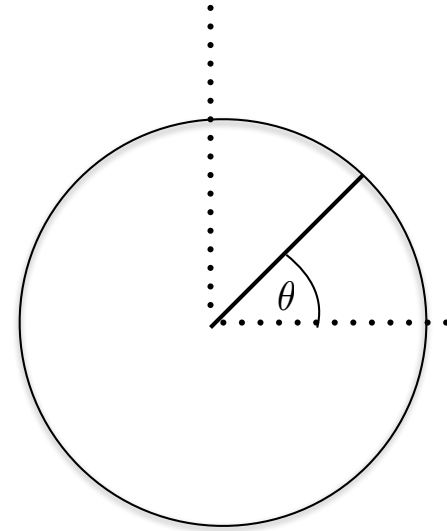
Galaxy-Galaxy Lensing

Theorem:

In polar coordinates

$$\kappa(r,\theta) = \frac{1}{2}\nabla^2\phi = \frac{1}{2}\left(\frac{\partial^2}{\partial r^2} + \frac{1}{r}\frac{\partial}{\partial r} + \frac{1}{r^2}\frac{\partial}{\partial\theta}\right)\phi(r,\theta) \qquad \text{convergence}$$

$$\gamma_t(r,\theta) = -\frac{1}{2}\left(\frac{\partial^2}{\partial r^2} - \frac{1}{r}\frac{\partial}{\partial r} - \frac{1}{r^2}\frac{\partial^2}{\partial\theta^2}\right)\phi(r,\theta) \qquad \text{tangential shear}$$

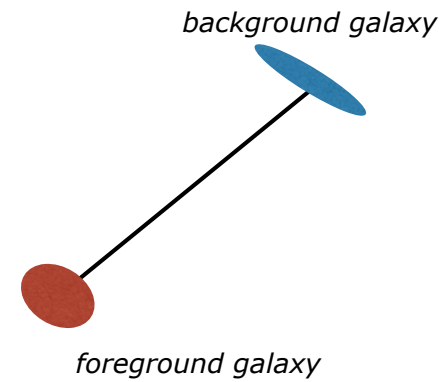Adding these two equations gives

Theorem:

$$\langle\gamma_t\rangle = \overline{\kappa} - \langle\kappa\rangle$$

Tangential shear averaged around a circle on the sky

Convergence averaged within the circle

Convergence averaged around a circle on the sky

Galaxy-Galaxy Lensing

background galaxy

foreground galaxy

In the weak lensing regime the tangential shear can be measure with the ellipticity of galaxies. This formula can be applied to the correlation between the tangential ellipticity of a background galaxy with respect to the position of foreground galaxies. If $\vec{x}_i$ are the positions of the foreground objects and $\vec{y}_j$ are the positions of the background galaxies then

$$\langle \gamma_t \rangle (r) = \overline{\kappa}(r) - \langle \kappa \rangle (r) \simeq \frac{1}{N} \sum_{r-\delta < |x_i - y_j| < r+\delta} \epsilon_t^i$$

Because the sources and lenses are at all different distances this is often rescaled to a standard source and lens redahift and the result given as a function of the physical size on this lens plane

$$\Delta\Sigma(R) \simeq \frac{1}{N\Sigma(\overline{z}_l, \overline{z}_s)} \sum_{R-\delta < |x_i - y_j| D_s < R+\delta} \epsilon_t^i \, \Sigma_{\mathrm{crit}}(z_i, z_j)$$

Weights for each pair are usually also included to miximize the signal-to-noise in this quantity, but I'll leave those out.

Galaxy-Galaxy Lensing

Measurements

background galaxy

foreground galaxy

Break galaxy sample up into foreground and background samples using redshift or colours.

Further break the sample up according foreground galaxies's properties - LRGs etc.

Proposed by Tyson et al. 1984

weak detection Brainerd, et al 1996

detection in the Sloan Digital Sky Survey (SDSS) Fisher et al. 2000

Mandelbaum, at al. 2013 SDSS
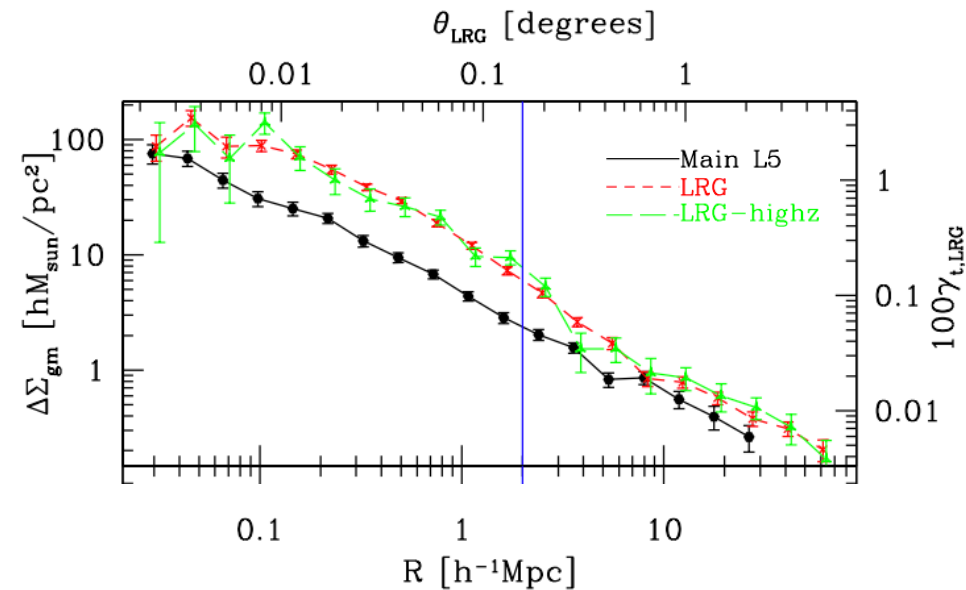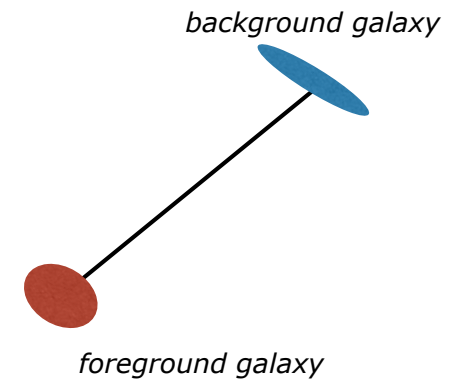
Galaxy-Galaxy Lensing Measurements

Break galaxy sample up into foreground and background samples using redshift or colours

Further break the sample up according to foreground galaxies's properties. LRGs etc.

Proposed by Tyson et al. 1984

weak detection Brainerd, et al 1996

detection in the Sloan Digital Sky Survey (SDSS) Fisher et al. 2000

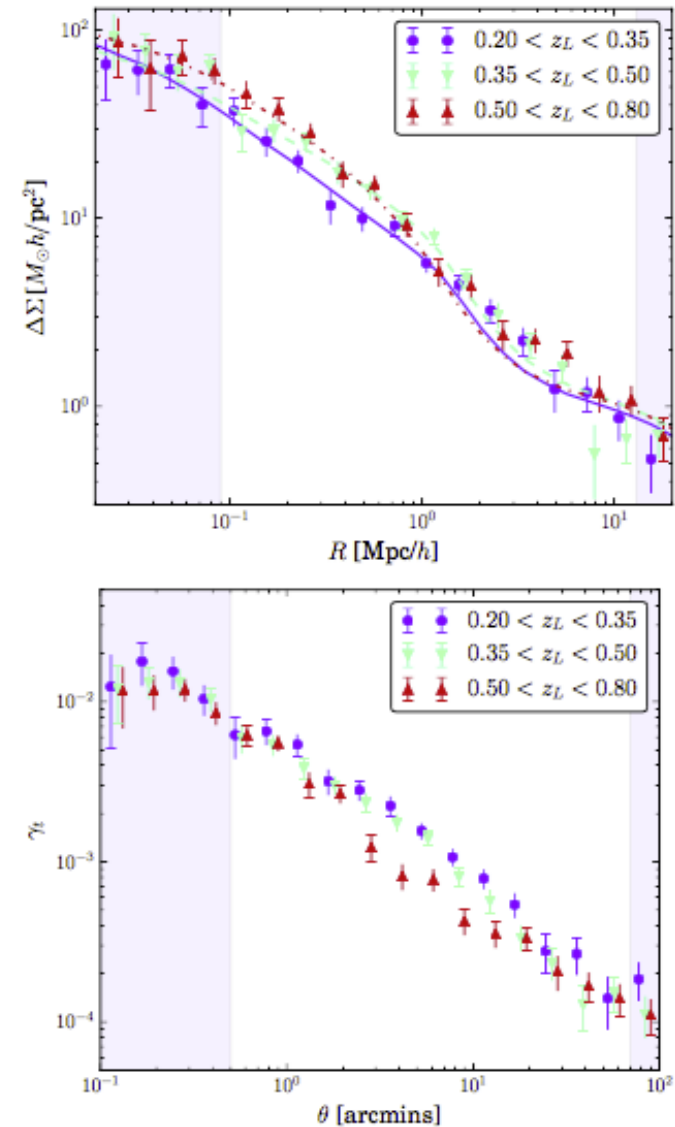## DES Data
Clampitt et al. 2017

Figure 7. (*upper panel*): $\Delta\Sigma$ measurement and statistical error bars for redMaGiC lenses in three redshift bins (as labelled). Best-fit model curves are also shown for each sample. The three different lens bins are consistent within our errors. (*lower panel*): The same, but showing the tangential shear γ_t.

Galaxy-Galaxy Lensing Measures:

- *the mass of a galaxies + halos at larger radii and smaller sizes than strong lensing - several kpc to Mpc distances*

- *the dark matter density profile around galaxies*

- *Mass-to-light ratios of galaxies, bias*

- *evolution in these with time*

- *Correlation of mass with other properties of the galaxies*

- *By comparing Galaxy-galaxy lensing to the galaxy velocity correlation function you can test General Relativity Reyes, et al. 2010, Nature*

Zu & Mandelbaum, 2014 SDSS

Linking Stellar to Dark Matter 15
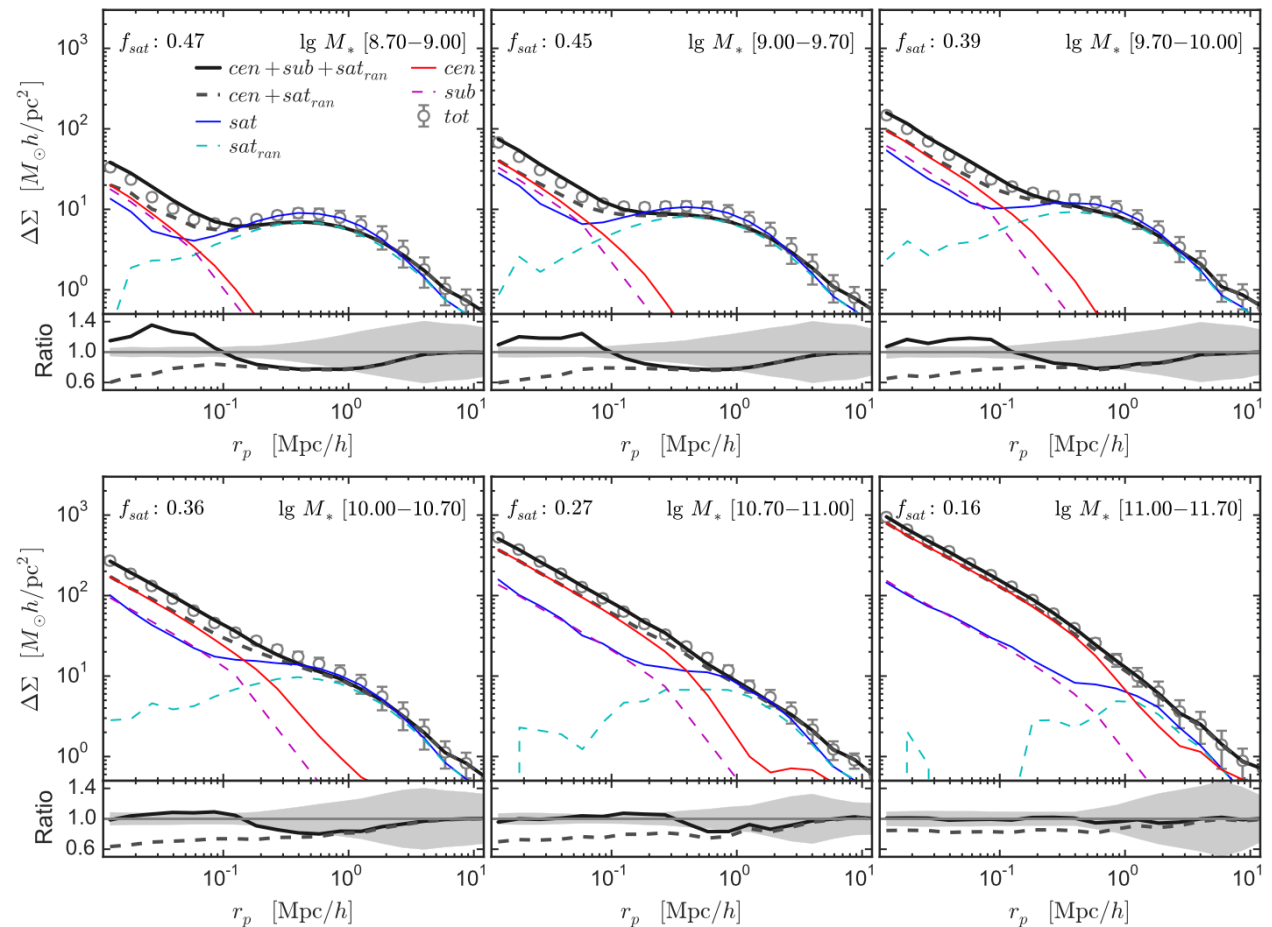
$$D_s \vec{\beta} = D_s \vec{\theta} - \sum_i D_{si} \hat{\alpha}_i \left(\vec{x}_i \right)$$
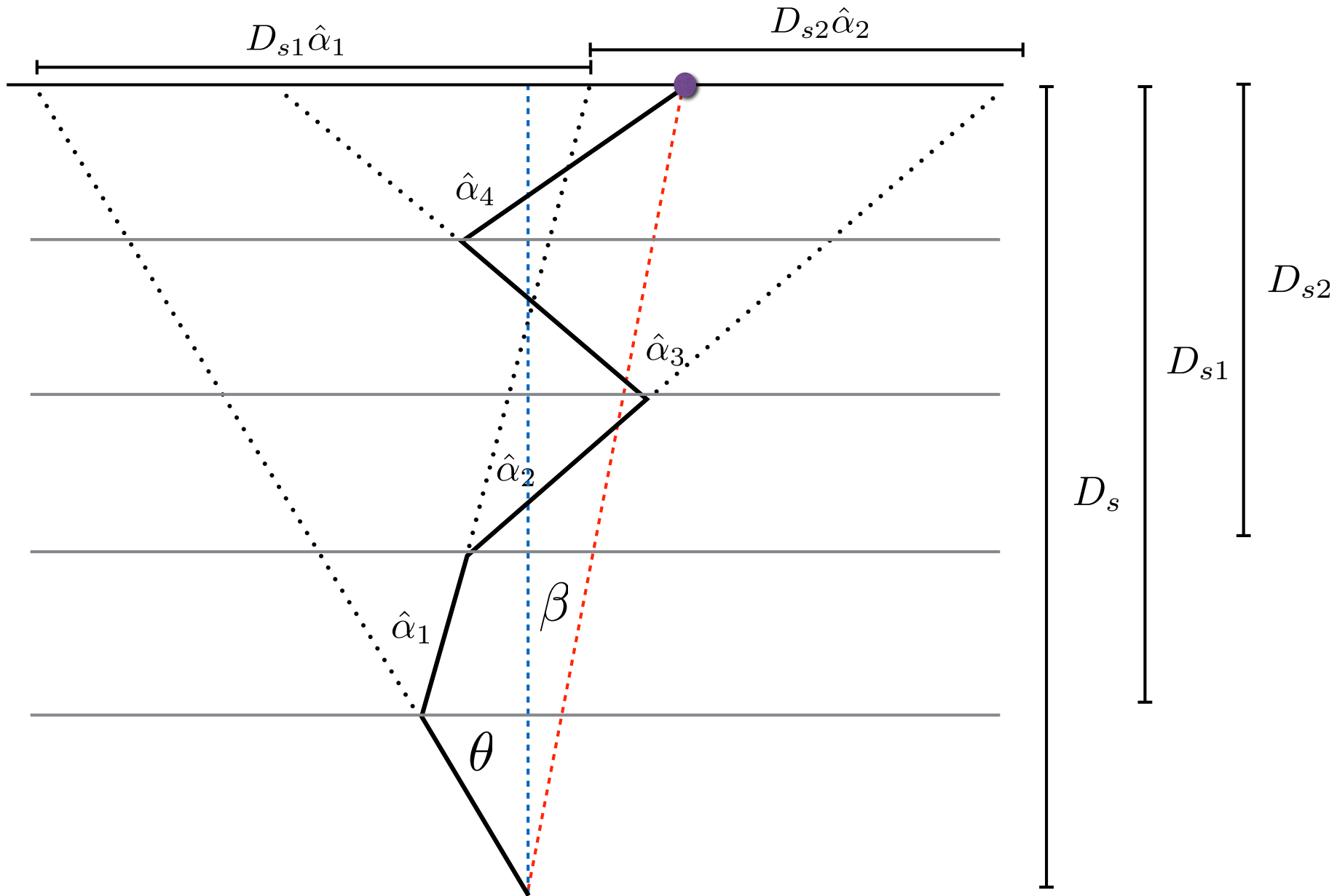
Multiplane Lensing Equation

$$ds^2 = g_{\nu\mu}dx^\nu dx^\mu = c^2 dt^2 - a(t)^2 \left[d\chi^2 + f^2(\chi)d^2\Omega \right]$$

$$D_{12} = af(\chi_2 - \chi_1)$$

$$\vec{\beta} = \vec{\theta} - \frac{1}{D_s} \sum_i D_{si}\hat{\alpha}_i\left(\vec{x}_\perp, \chi\right) \tag{51}$$

deflection by a thin slab
$$= \vec{\theta} - \frac{2}{D_s} \sum_i D_{si}\delta\chi\nabla_\perp\phi\left(\vec{x}_\perp, \chi\right) \tag{52}$$

turn the sum over slabs into an integral
$$= \vec{\theta} - \frac{2}{D_s} \int d\chi \, D_{si}\nabla_\perp\phi\left(\vec{x}_\perp, \chi\right) \tag{53}$$

from expression for angular size distance
$$= \vec{\theta} - 2\int d\chi \, \frac{f(\chi_s - \chi)}{f(\chi_s)}\nabla_\perp\phi\left(\vec{x}_\perp, \chi\right) \tag{54}$$

$$\kappa = -\frac{1}{2}\left(\frac{\partial\beta_1}{\partial\theta_1} + \frac{\partial\beta_2}{\partial\theta_2} \right) \tag{55}$$

The definitions of the convergence and shear components in terms of derivatives of the angles

$$\gamma_1 = -\frac{1}{2}\left(\frac{\partial\beta_1}{\partial\theta_1} - \frac{\partial\beta_2}{\partial\theta_2} \right) \tag{56}$$

$$\gamma_2 = -\frac{\partial\beta_1}{\partial\theta_2} \stackrel{?}{=} -\frac{\partial\beta_2}{\partial\theta_1} \tag{57}$$

$$\frac{\partial\beta_1}{\partial\theta_2} \neq \frac{\partial\beta_2}{\partial\theta_1}$$
This means there is a rotation. This is not possible in the case of a thin single plane lens.

$$\frac{\partial\beta_i}{\partial\theta_j} = \delta_{ij} - 2\int d\chi \, \frac{f(\chi_s - \chi)}{f(\chi_s)}\left[\frac{\partial x_k}{\partial\theta_j} \right]\frac{\partial^2\phi}{\partial x_k \partial x_i}\left(\vec{x}_\perp, \chi\right) \tag{58}$$

What it this? The position on each plane depends on the deflections on all previous planes so taking this derivative is not trivial.

Multiplane Lensing Equation

The Born Approximation:

- *Calculate the deflections on each plane at the positions the unperturbed path would have taken.*

- *This is not valid at small scales and when there is one or more not so weak perturbers along the line of sight.*

$$D_s \vec{\beta} = D_s \vec{\theta} - \sum_i D_{si} \hat{\alpha}_i \left(\vec{x}_i \right)$$

Remember that the angular size distance is

$$\left[\frac{\partial x_k}{\partial \theta_j} \right] = f(\chi) \delta_{jk}$$
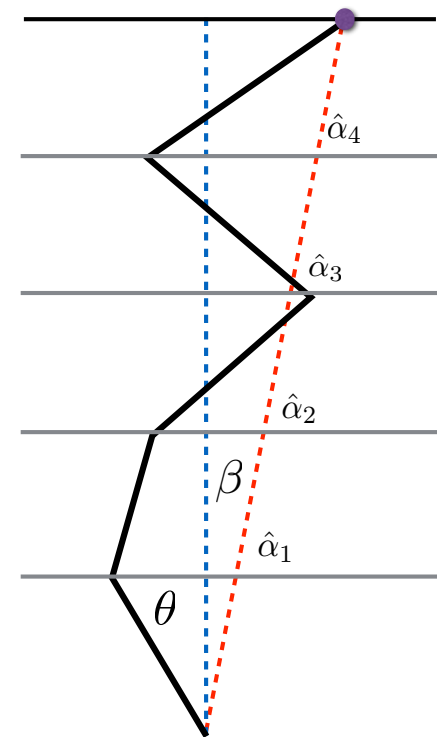
$$D(z) = a(z) f(\chi) = \frac{f(\chi)}{(1+z)}$$

$$\frac{\partial \beta_i}{\partial \theta_j} = \delta_{ij} - 2 \int d\chi \left[\frac{f(\chi_s - \chi) f(\chi)}{f(\chi_s)} \right] \frac{\partial^2 \phi}{\partial x_j \partial x_i} \left(\vec{x}_\perp, \chi \right)$$

convergence

$$\kappa(\vec{\theta}) = 2 \int_0^{\chi_s} d\chi \left[\frac{f(\chi_s - \chi) f(\chi)}{f(\chi_s)} \right] \nabla^2_\perp \phi \left(\vec{x}_\perp, \chi \right) \big|_{\vec{x}_\perp = f(\chi) \vec{\theta}}$$

Multiplane Lensing Equation

$$\nabla_\perp^2 \phi = \nabla^2 \phi - \partial_\parallel^2 \phi$$

$$\nabla^2 \phi = 4\pi G \bar{\rho} a^2 \; \delta = \frac{4\pi G \bar{\rho}_o}{a} \; \delta = \frac{3}{2} H_o^2 \frac{\Omega_m}{a} \; \delta$$

from perturbation theory the Poisson equation relating the potential to the density contrast

$$\kappa(\vec{\theta}) = \frac{3}{2} \frac{H_o^2 \Omega_m}{c^2} \int_0^{\chi_s} d\chi \; \frac{1}{a(\chi)} \left[\frac{f(\chi_s - \chi) f(\chi)}{f(\chi_s)} \right] \delta(\vec{\theta})$$

$$= \int_0^{\chi_s} d\chi \; a(\chi) \; \frac{\bar{\rho} \delta(\vec{\theta})}{\Sigma_{\mathrm{crit}}(\chi, \chi_s)}$$

Essentially it is a sum of the surface density contrasts with respect to the average density of the Universe - assuming 1) weak lensing, 2) Born Approximation

The source galaxies are not at a single redshift so usually one measures the convergence map averaged over the source galaxy redshift distribution.
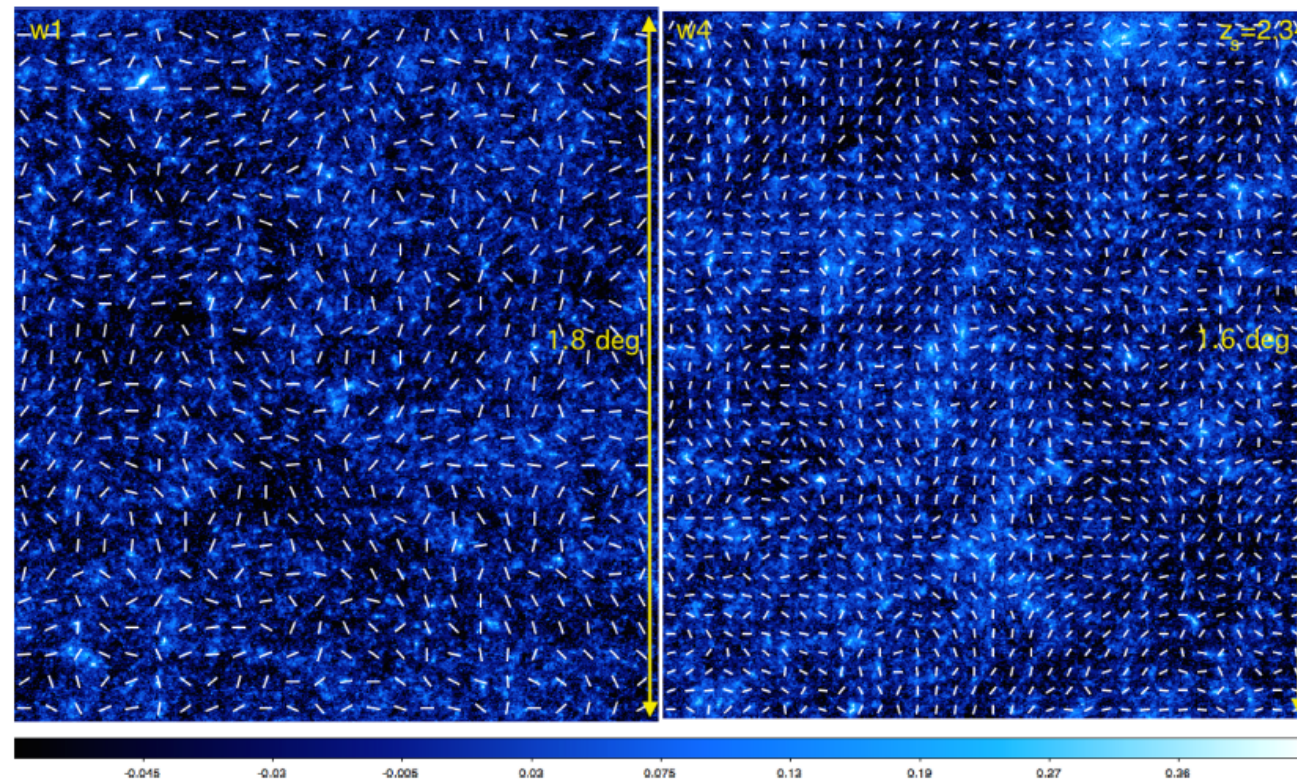
$$\kappa_g(\vec{\theta}) = \int_0^\infty d\chi_s \, g(\chi_s) \kappa(\vec{\theta})$$

$$= \frac{3}{2} \frac{H_o^2 \Omega_m}{c^2} \int_0^\infty d\chi \frac{1}{a(\chi)} \left[\int_\chi^\infty d\chi_s \; g(\chi_s) \frac{f(\chi_s - \chi) f(\chi)}{f(\chi_s)} \right] \delta(\vec{\theta}, \chi)$$

$$= \frac{3}{2} \frac{H_o^2 \Omega_m}{c^2} \int_0^\infty d\chi W_{\mathrm{eff}}(\chi) \delta(\vec{\theta}, \chi)$$

For a distribution of galaxies with different distances.
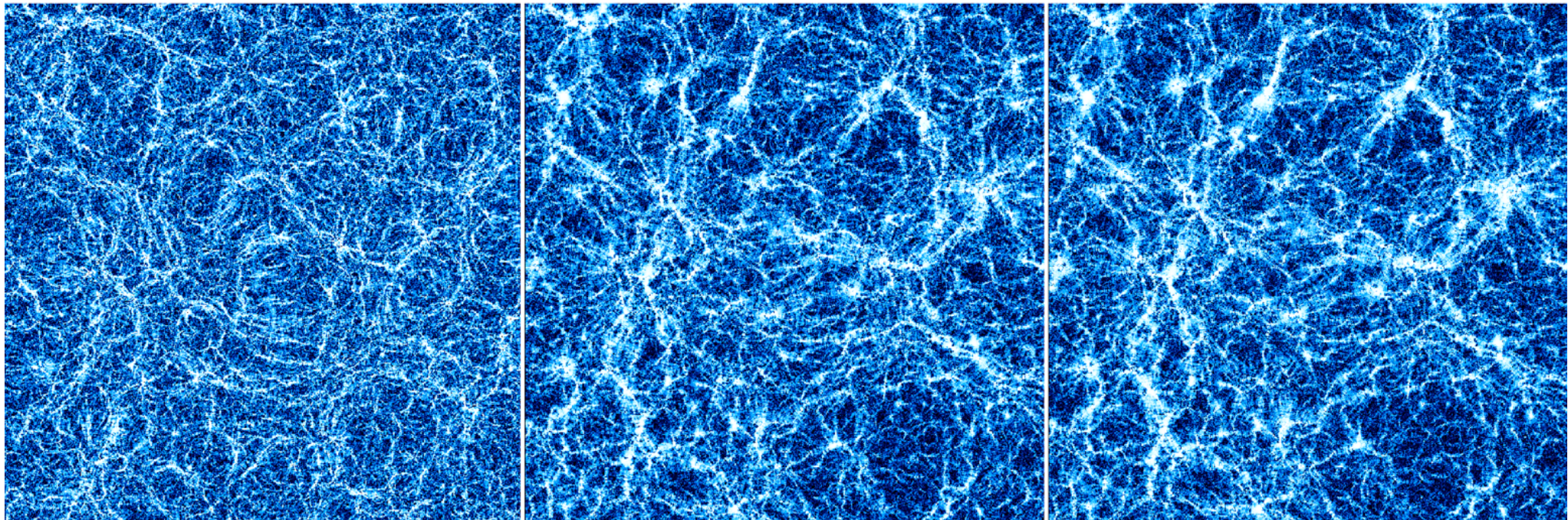
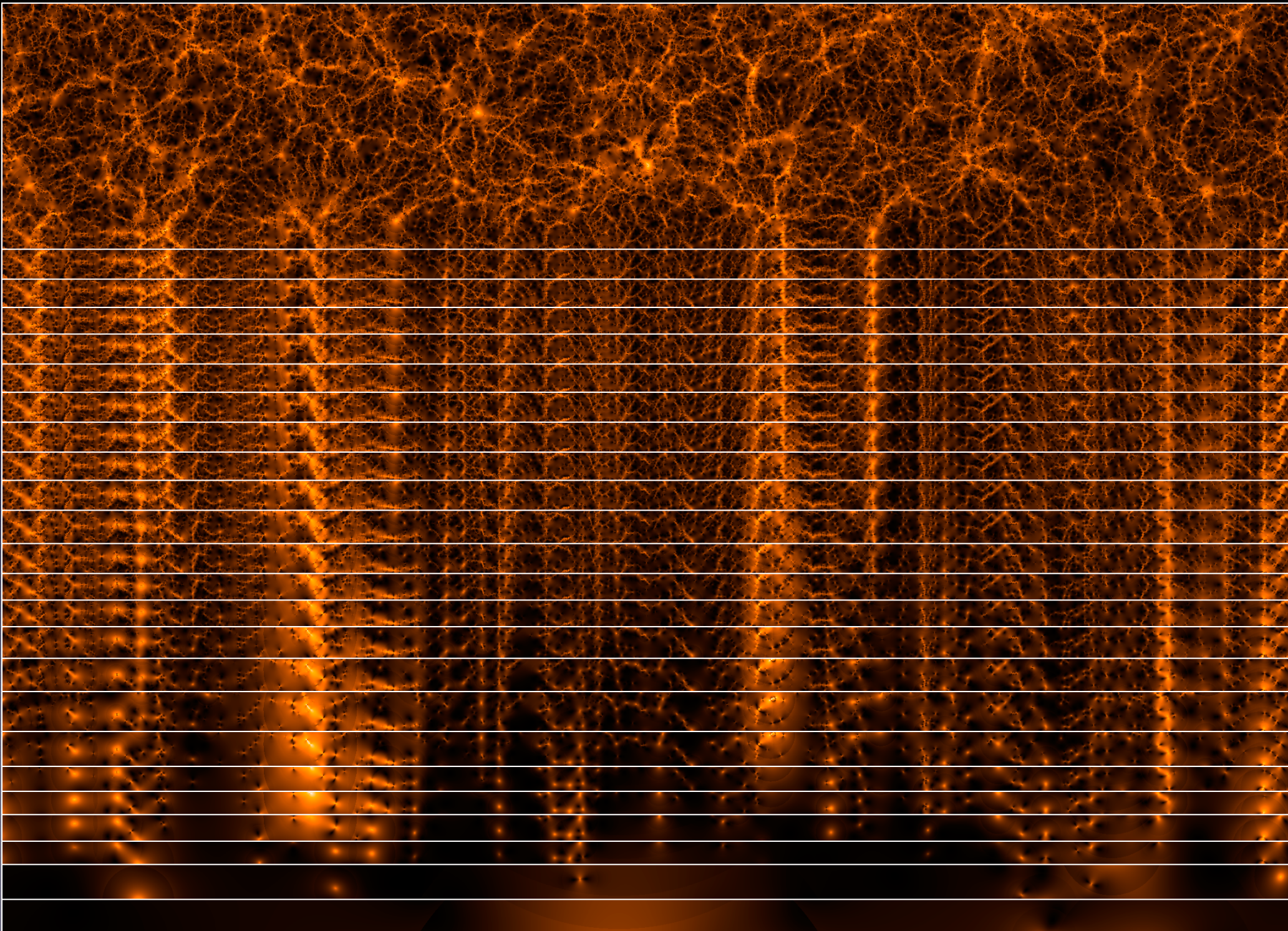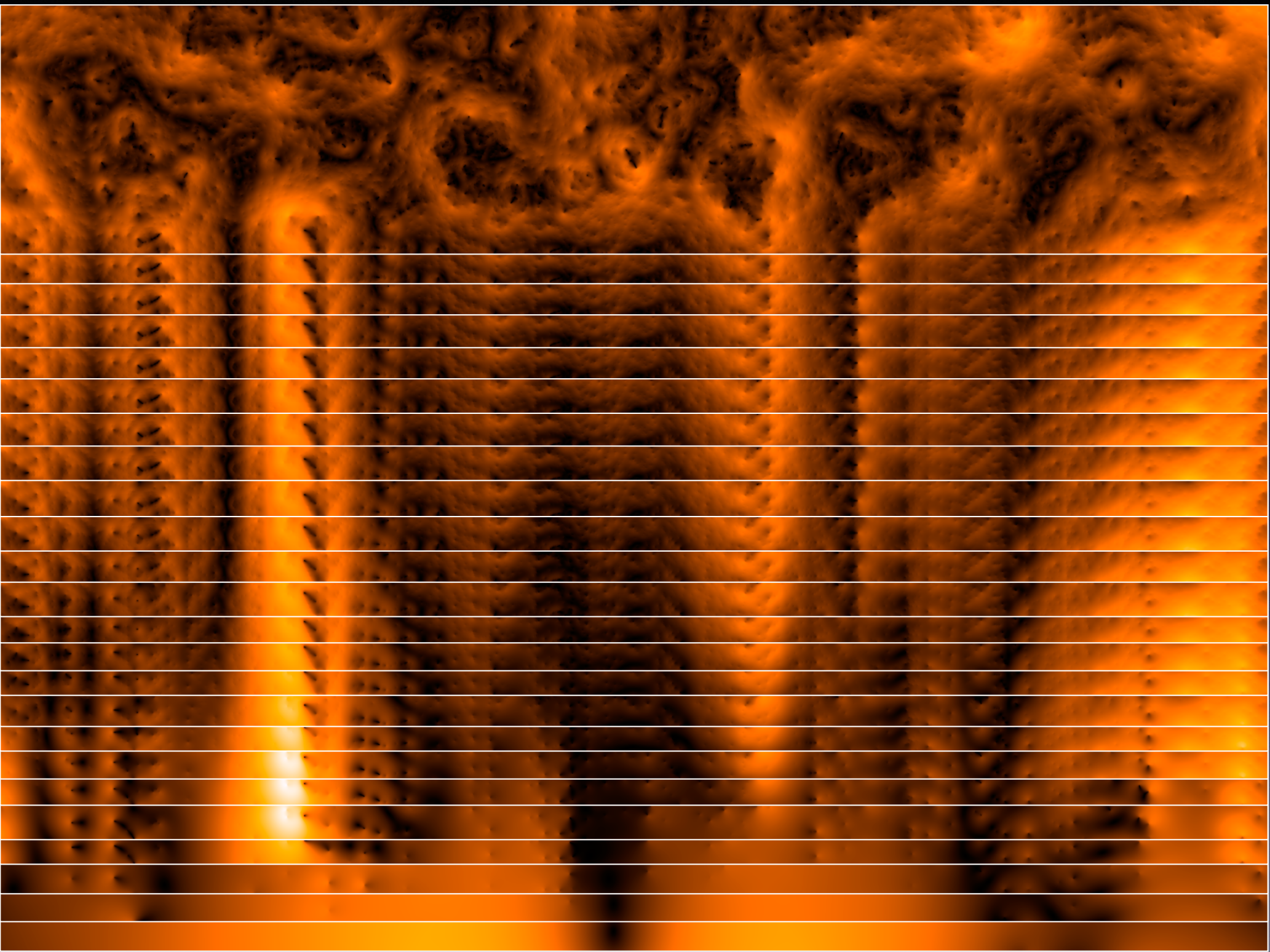convergence map as a function of source redshift
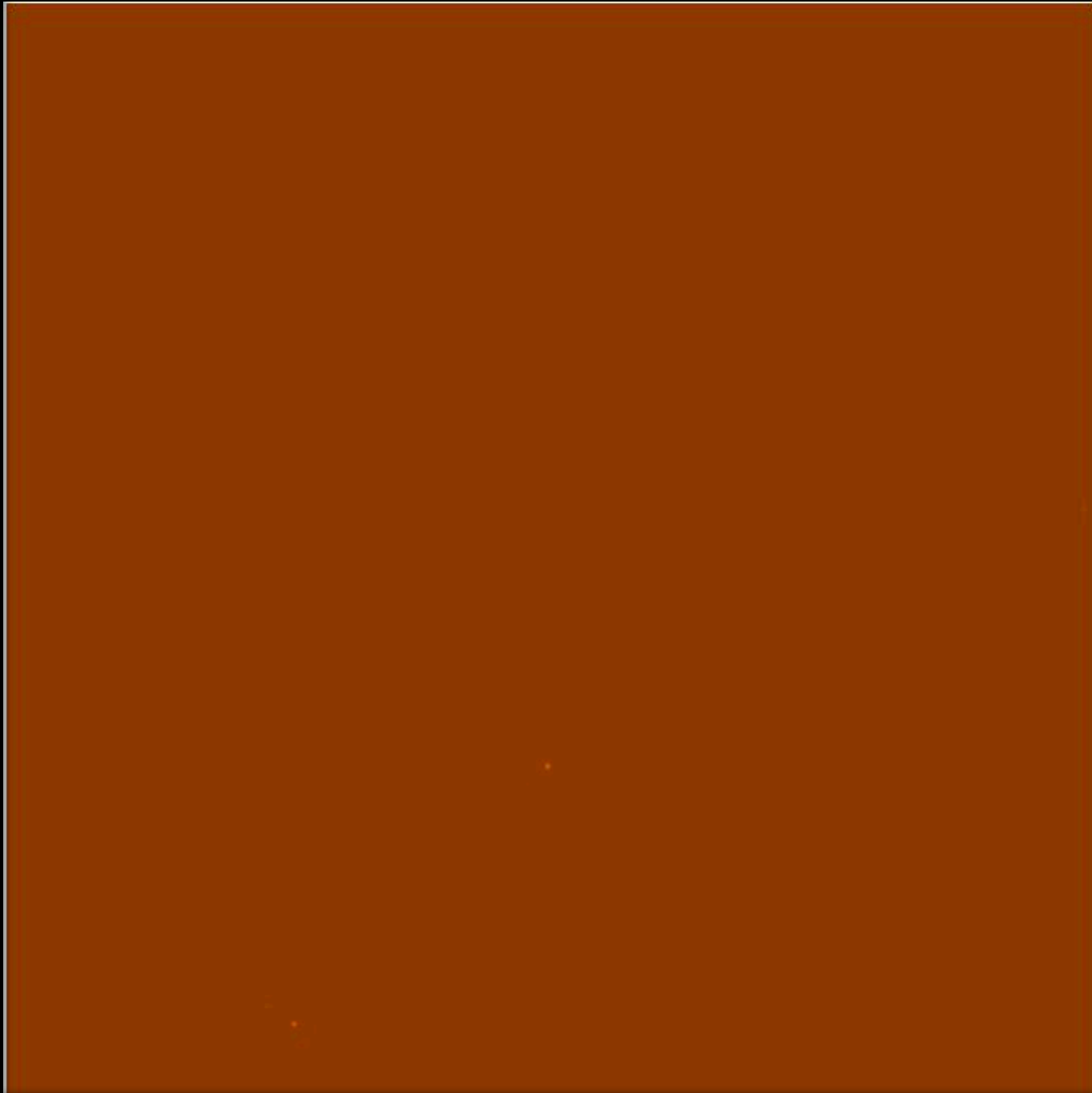
Carlo Giocoli & RBM, 2016

Convergence maps with shear overlaid

From ray-tracing simulation
using the MultiDark cosmological simulation
Giocoli et al. 2016

maps of the magnitude of the shear

The Power Spectra

Convergence

$$\tilde{\kappa}(\vec{\ell}) = \int d^2\theta e^{+i\vec{\theta}\cdot\vec{\ell}}\kappa(\vec{\theta})$$

$$\langle \kappa(\vec{\ell})\kappa(\vec{\ell}')^* \rangle = (2\pi)^2\delta^2(\vec{\ell} - \vec{\ell}')P_\kappa(\ell)$$

The convergence and density power spectra can be related with the Limber approximation in Fourier space (Kaiser 1992)

$$P_\kappa(\ell) = \left[\frac{3}{2}\frac{H_o^2\Omega_m}{c^2}\right]^2 \int d\chi \frac{1}{\chi^2}\left[\frac{f(\chi_s - \chi)f(\chi)}{a(\chi)f(\chi_s)}\right]^2 P_\delta\left(k = \frac{\ell}{\chi}, \chi\right)$$

This is the approximation that it is only the perpendicular distance between points in space that contributes to the angular correlations. It is generally a good approximation, but for high precision work it must be dropped. We have also taken small angle / flat sky approximation that allows us to take the Fourier transformations on the sky. This will break down at large angular scales. A more rigorous treatment uses spherical harmonics instead of a Fourier transform, but it less intuitive.

Cosmological Background

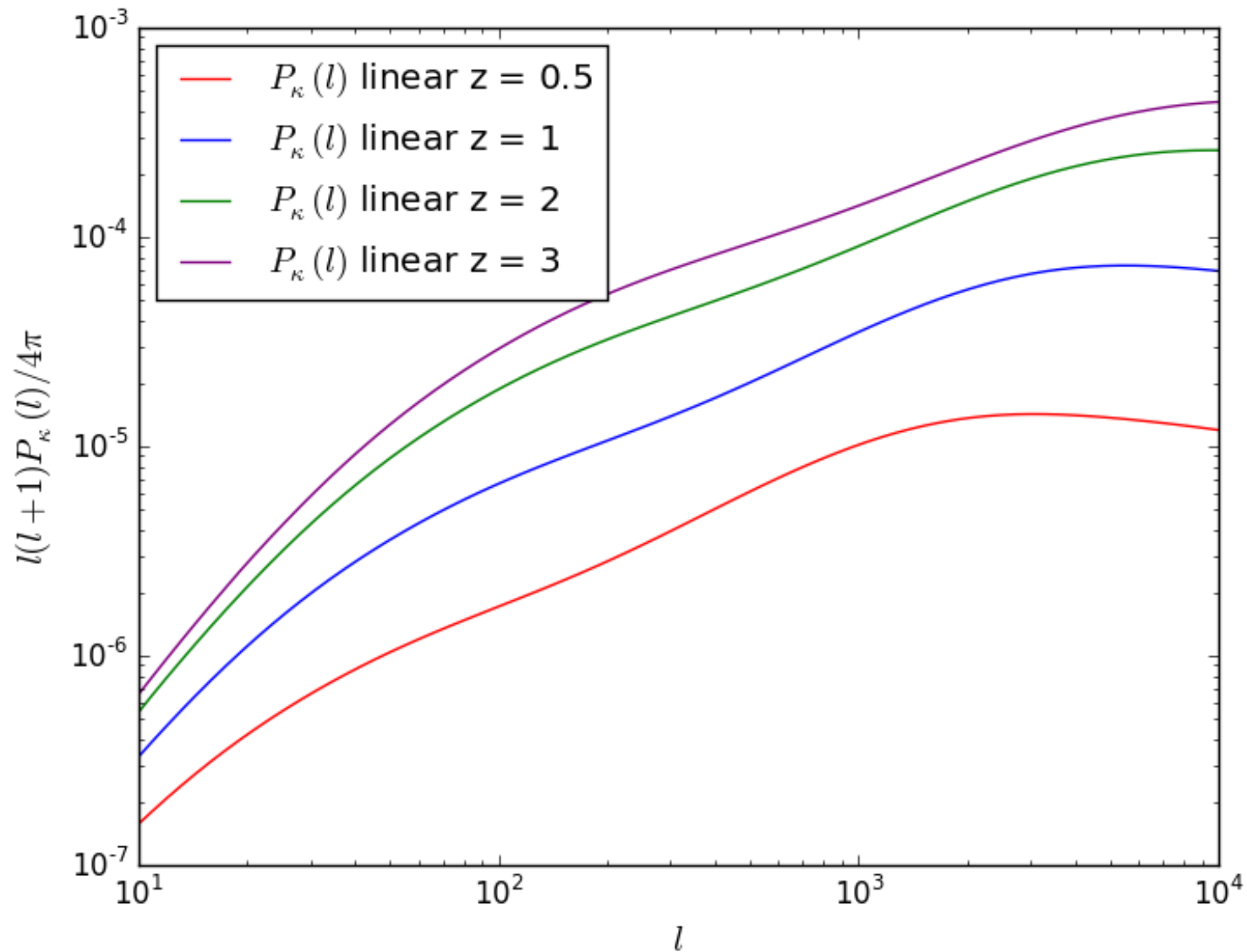power spectrum of density fluctuations for different redshifts
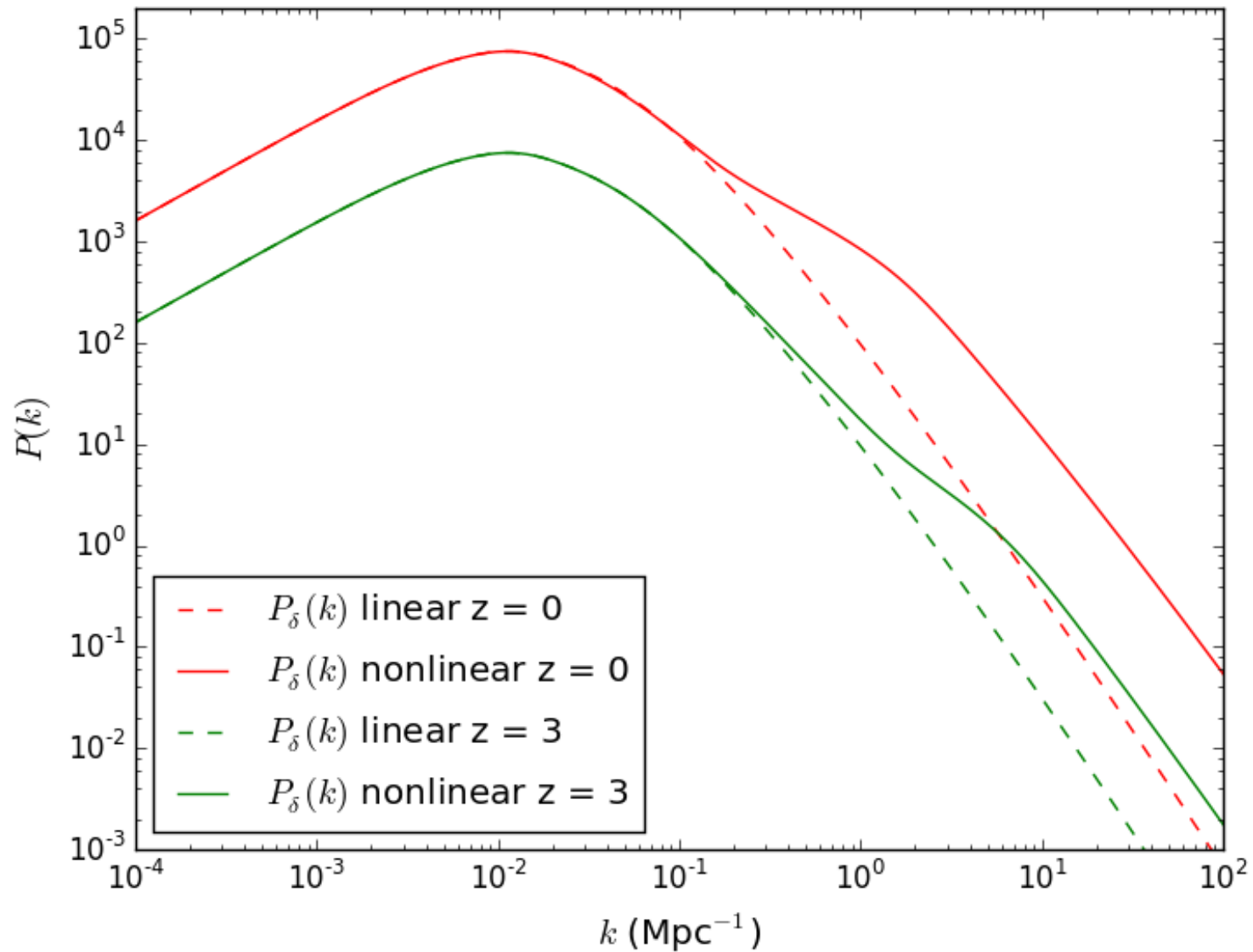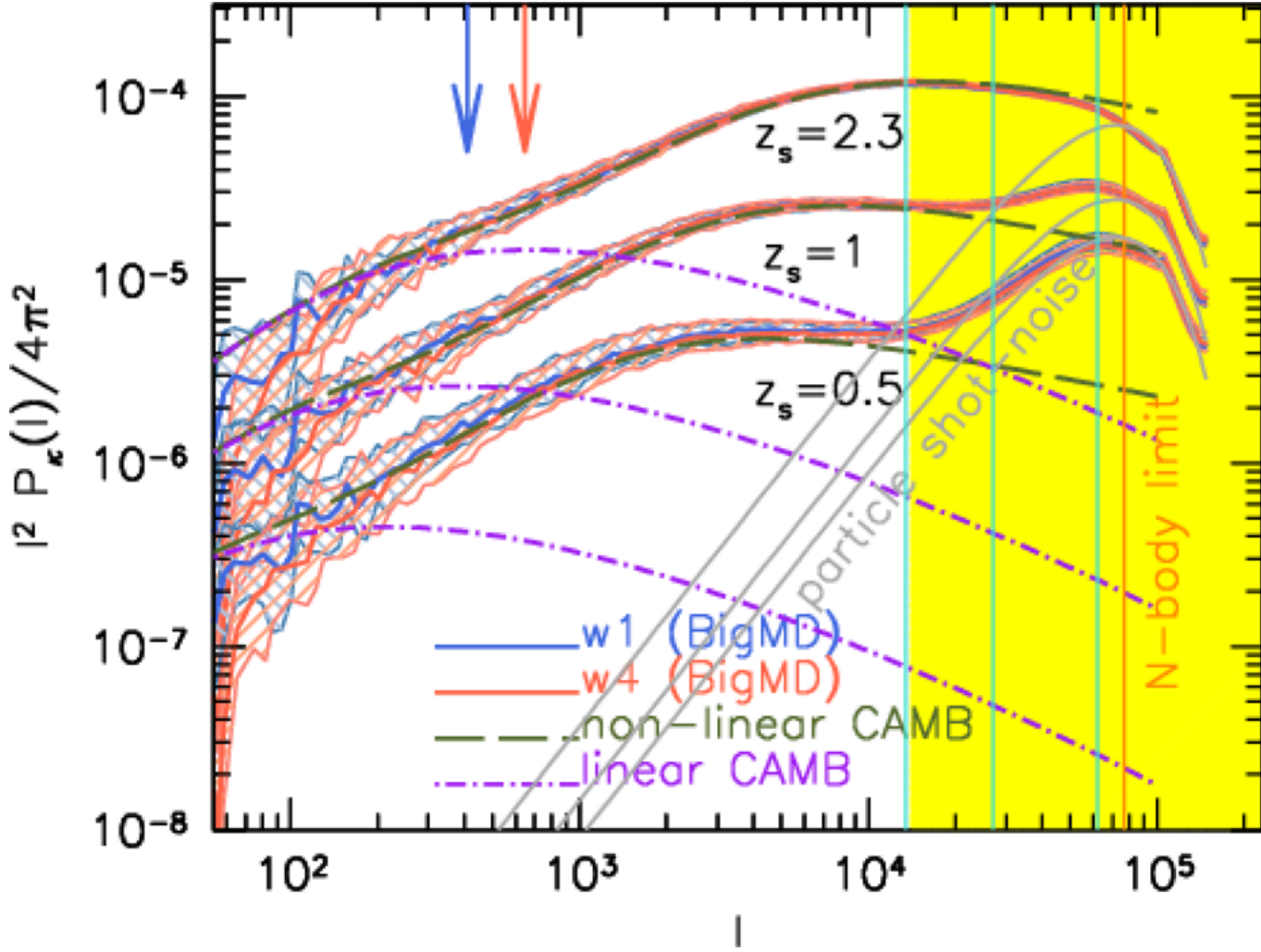
Cosmological Background

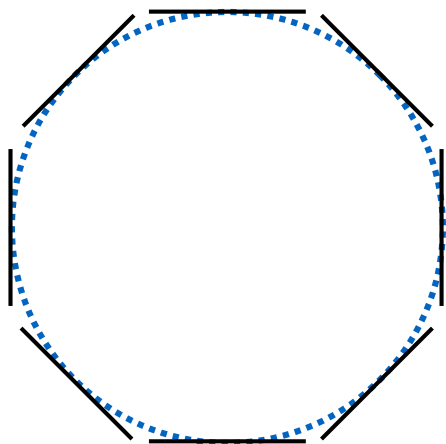Convergency power spectrum for different source redshifts

Cosmological Background

From ray-tracing simulation
using the MultiDark cosmological simulation
Giocoli et al. 2016

Observing Cosmic Shear

E-modes

$\gamma_t > 0$
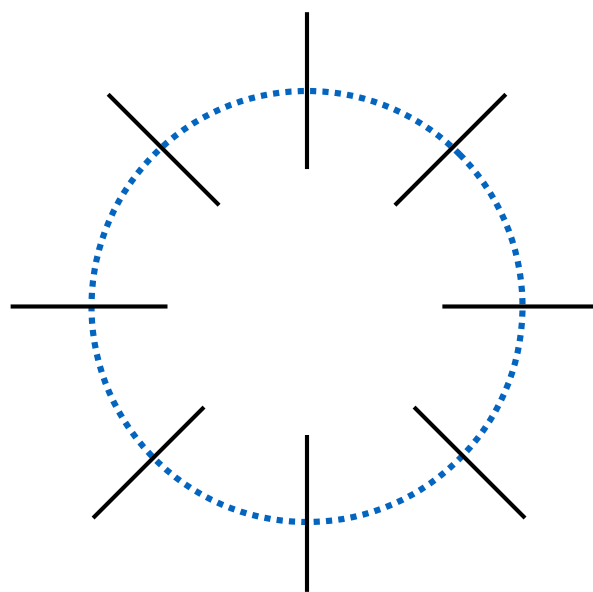
$\gamma_t < 0$

B-modes
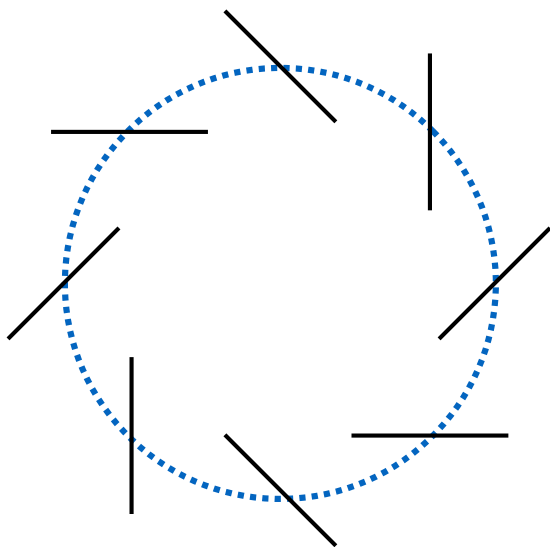
$\gamma_\times < 0$

$\gamma_\times > 0$
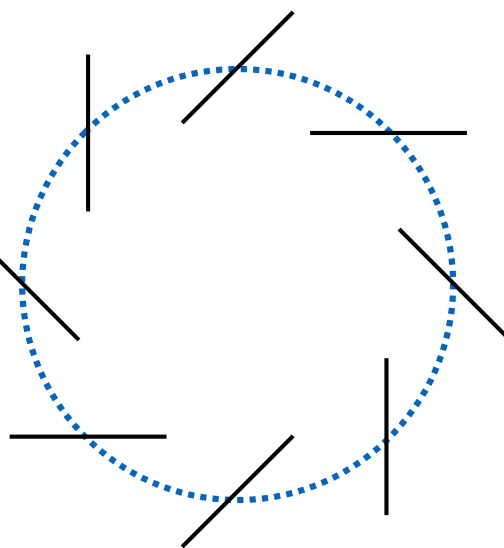
Observing Cosmic Shear

E and B mode decomposition

Can decompose any 2D vector field into a E and B components

deflection $\quad \alpha_i = \partial_i \phi^E + \epsilon_i^j \partial_j \phi^B \qquad \epsilon = \begin{pmatrix} 0 & 1 \\ -1 & 0 \end{pmatrix} \qquad \partial_i \equiv \dfrac{\partial}{\partial \theta_i}$

$$\partial_{ij} \equiv \frac{\partial^2}{\partial \theta_i \partial \theta_j}$$

shear field - traceless part of the shear tensor

$$\gamma_{ij} \equiv \partial_i \alpha_j - \frac{\delta_{ij}}{2} \mathrm{tr}\left[\partial_i \alpha_j\right] = \left[\partial_{ij} - \frac{\delta_{ij}}{2}\nabla^2\right]\phi^E + \left[\epsilon_i^k \partial_{kj} + \epsilon_j^k \partial_{ki}\right]\phi^B$$

$$\gamma_{12} \neq \gamma_{21} \qquad rotations$$
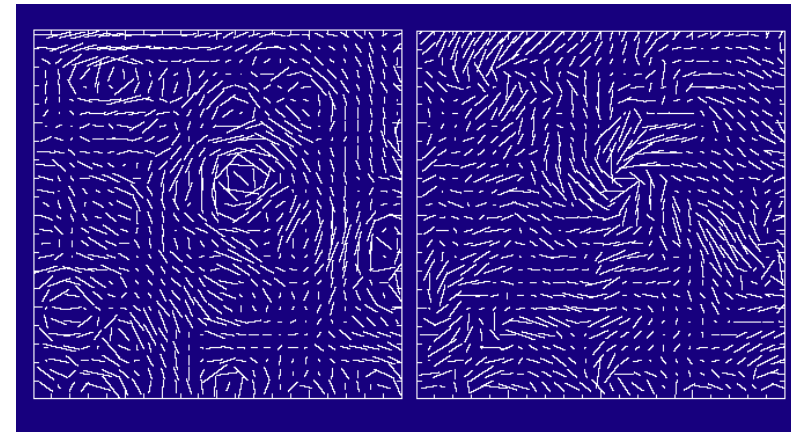
Sources of B-modes

- *Breakdown of Born Approximation and the weak lensing approximation (nonlinear terms)*

- *Nonlinear terms in the relation between the shear estimator and the shear*

- *Bias in the galaxy selection*

- *Correlations in the intrinsic shape of galaxies*

- *residuals in the PSF (point spread function) corrections*

Observing Cosmic Shear

The Aperture Mass

$$M_{ap}(\Theta, \vec{\theta}_o) = \int d^2\theta \; \gamma_t(\vec{\theta}) \, Q\left(\frac{|\vec{\theta} - \vec{\theta}_o|}{\Theta}\right)$$

$$= \int d^2\theta \; \kappa(\vec{\theta}) \, U\left(\frac{|\vec{\theta} - \vec{\theta}_o|}{\Theta}\right)$$

tangential and cross shear with respect to the centre of the aperture mass

$$\int_0^\infty dx \, x \, U(x) = 0 \qquad Q(x) = \frac{2}{x^2} \int_0^x dx' \, x' \, U(x') - U(x)$$

$$\gamma_t = -\gamma_1 \cos(2\phi_o) - \gamma_2 \sin(2\phi_o)$$
$$\gamma_\times = \gamma_1 \sin(2\phi_o) - \gamma_2 \cos(2\phi_o)$$

B-made aperture mass

$$M_{ap}^B(\Theta, \vec{\theta}_o) = \int d^\theta \; \gamma_\times(\vec{\theta}) \, Q\left(\frac{|\vec{\theta} - \vec{\theta}_o|}{\Theta}\right)$$

$$\langle M_{ap}(\Theta)^2 \rangle = \frac{\Theta^4}{2\pi} \int_0^\infty d\ell \, \ell \, P_\kappa^E(\ell) \left| \tilde{U}(\Theta\ell) \right|^2$$

$$\langle M_{ap}^B(\Theta)^2 \rangle = \frac{\Theta^4}{2\pi} \int_0^\infty d\ell \, \ell \, P_\kappa^B(\ell) \left| \tilde{U}(\Theta\ell) \right|^2$$

rms aperture mass is related to the related to power spectra

Observing Cosmic Shear

The Aperture Mass

Because the B-modes are expected to be very small, they are often used as a necessary, but not complete check on the systematic errors in the E-modes.
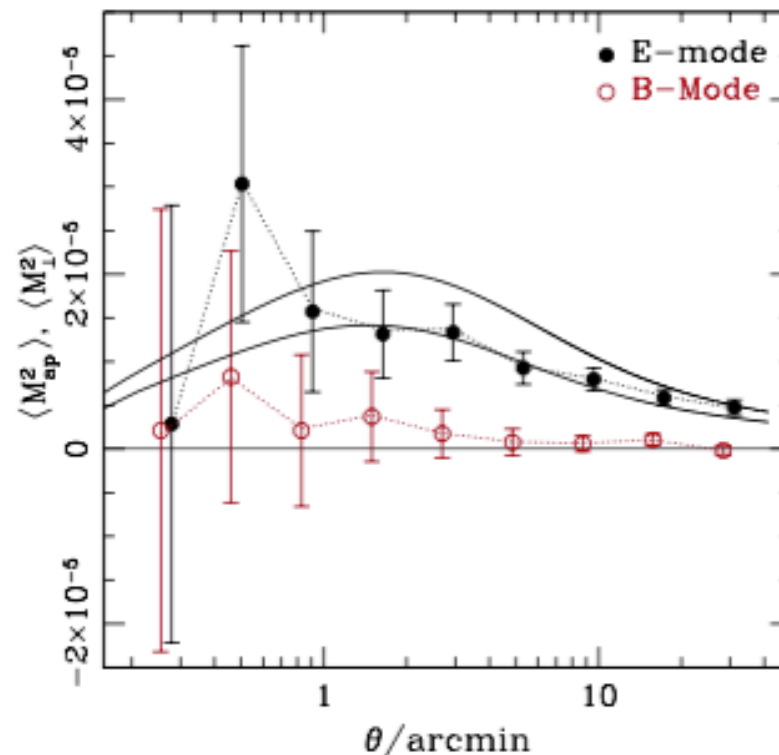
Figure 5. Aperture-mass dispersion measured in COSMOS. The two solid lines correspond to predictions with $\sigma_8 = 0.7$ and 0.8, respectively. From Schrabback et al. (2010). Figure reproduced with permission from Schrabback et al. (2010), *A&A*, **516**, A63. © ESO.

Observing Cosmic Shear

Shear Correlation Function

$$\gamma_{\parallel}^{(i)}\gamma_{\parallel}^{(j)} > 0$$

$$\gamma_{\parallel}^{(i)}\gamma_{\parallel}^{(j)} < 0$$

$$\gamma_{\wedge}^{(i)}\gamma_{\wedge}^{(j)} > 0$$

$$\gamma_{\wedge}^{(i)}\gamma_{\wedge}^{(j)} < 0$$
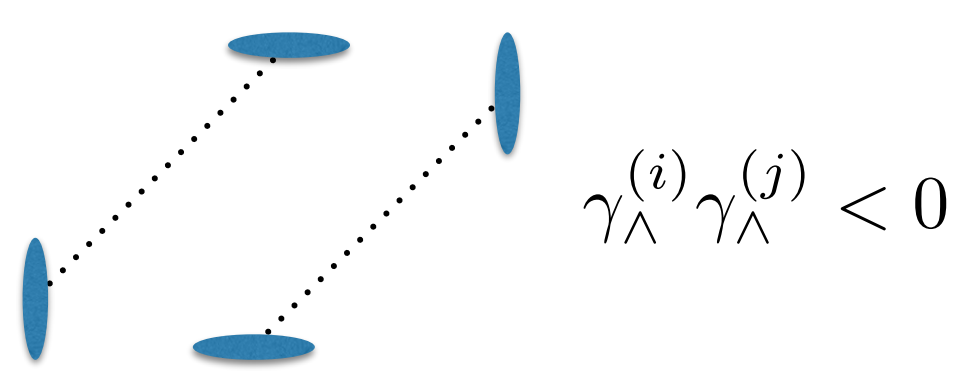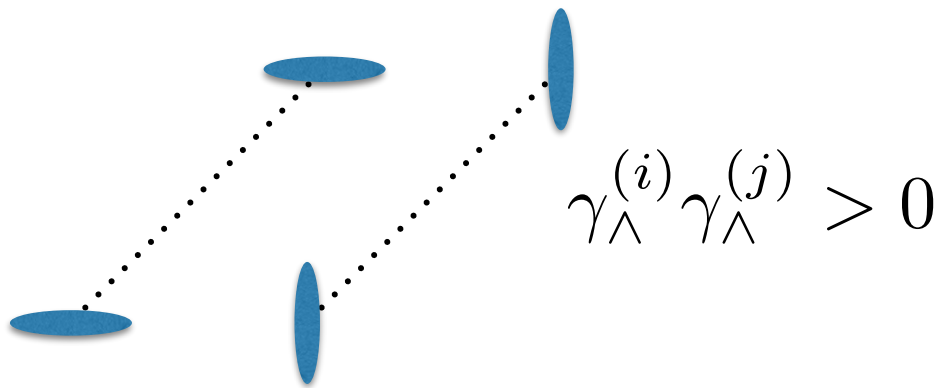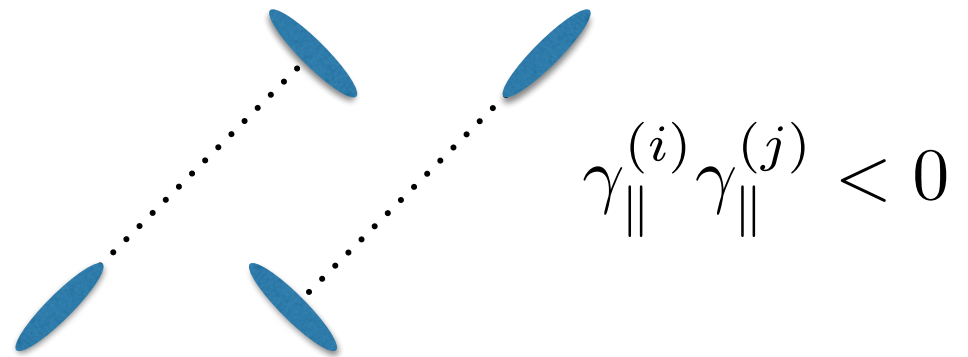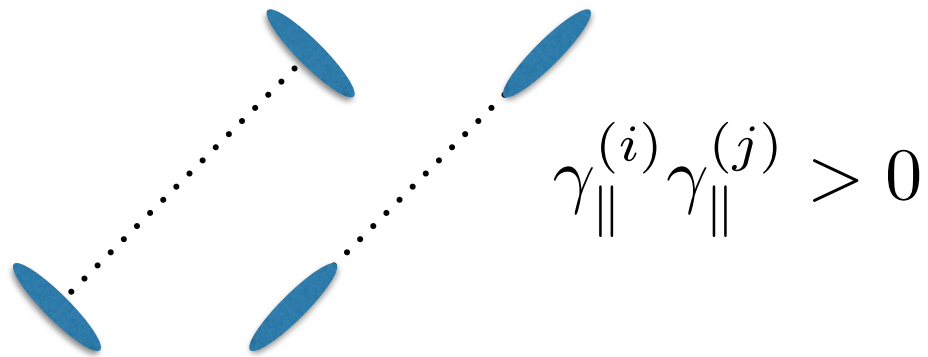
Observing Cosmic Shear

Shear Correlation Function

It is common to define the following two correlation functions

$$\xi_+ = \xi_\parallel + \xi_\wedge = \langle \gamma_1^{(i)} \gamma_1^{(j)} \rangle + \langle \gamma_2^{(i)} \gamma_2^{(j)} \rangle$$

$$\xi_- = \xi_\parallel - \xi_\wedge = \left[\langle \gamma_1^{(i)} \gamma_1^{(j)} \rangle - \langle \gamma_2^{(i)} \gamma_2^{(j)} \rangle \right] \cos(4\phi_{ij})$$

$$\langle \gamma_1^{(i)} \gamma_2^{(j)} \rangle = 0 \quad \text{by parity symmetry}$$

An estimators for these are

$$w_i \quad \text{Weights used to reduce the noise when the noise in each measured ellipticity is different.}$$

$$\hat{\xi}_\pm = \frac{\sum_{ij} w_i w_j \left[\epsilon_\parallel^{(i)} \epsilon_\parallel^{(j)} \pm \epsilon_\wedge^{(i)} \epsilon_\wedge^{(j)} \right]}{\sum_{ij} w_i w_j}$$

The sum is over all pairs of galaxies that are within range of separations.

Observing Cosmic Shear
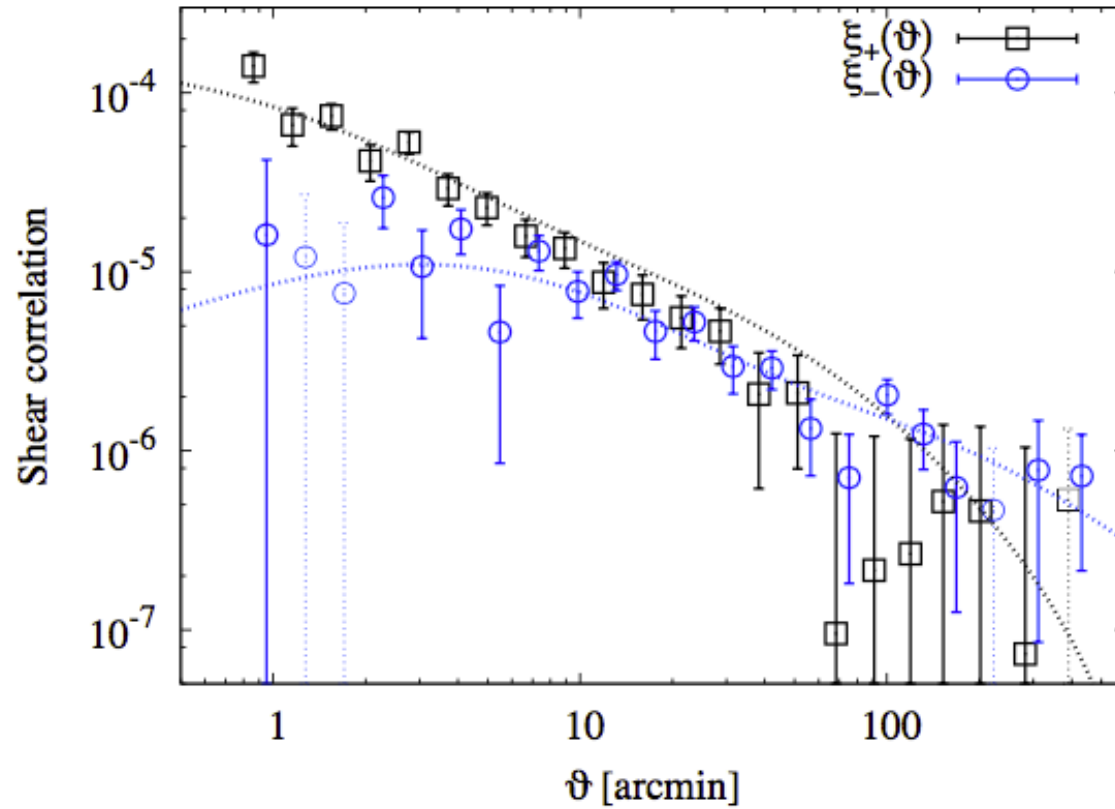
Figure 4. 2PCF components ξ_+ and ξ_- (32) measured in CFHTLenS. The d

Observing Cosmic Shear

Shear Correlation Function

No clear separation between E and B modes.

$$\xi_+(\theta) = \frac{1}{2\pi} \int d\ell \; \ell J_0(\ell\theta) \left[P_\kappa^E(\ell) + P_\kappa^B(\ell) \right]$$

$$\xi_-(\theta) = \frac{1}{2\pi} \int d\ell \; \ell J_4(\ell\theta) \left[P_\kappa^E(\ell) - P_\kappa^B(\ell) \right]$$

But pure E and B quantities can be constructed from them

$$X_{E,B} = \frac{1}{2\pi} \int_0^\infty d\ell \ell P_\kappa^{E,B}(\ell) W(\ell)$$

$$\hat{X}_{E,B} = \frac{1}{2} \sum_i \theta_i \Delta\theta_i \left[T_+ \hat{\xi}_+(\theta_i) \pm T_- \hat{\xi}_-(\theta_i) \right]$$

$$T_\pm(x) = \int_o^\infty ds \; s \; J_{0,4}(sx) W(s)$$

Observing Cosmic Shear

E & B mode decomposition
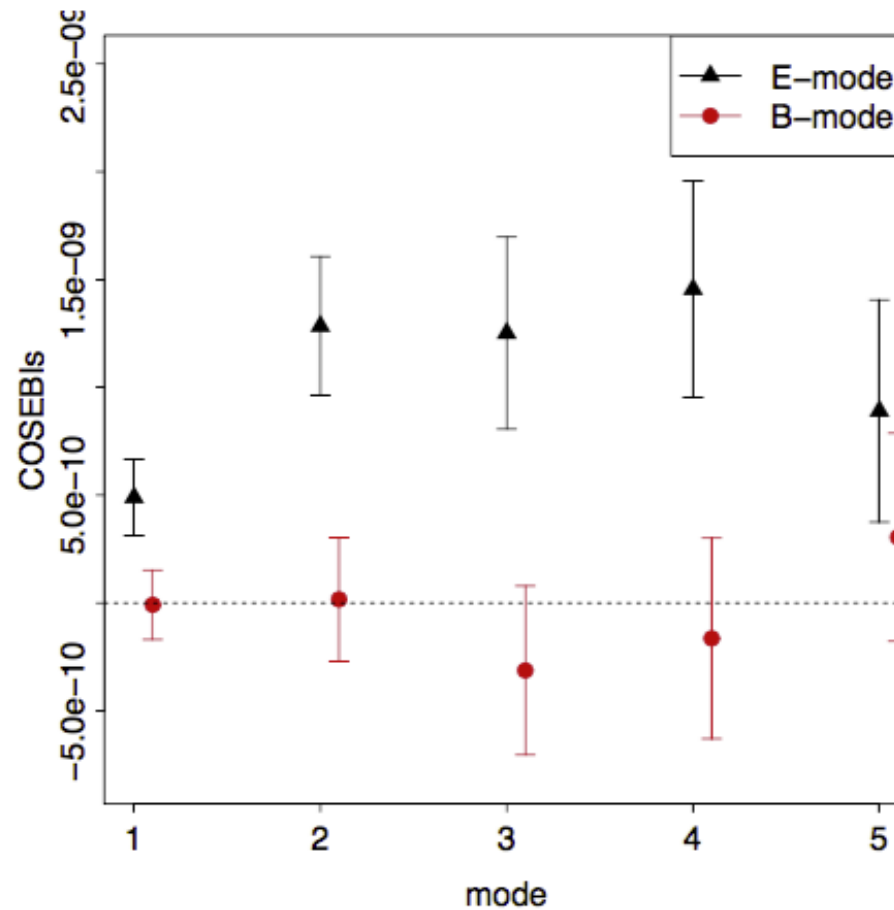
Figure 6. First five COSEBIs modes, measured in SDSS. From Huff et al. (2014a). Figure reproduced with permission from Huff et al. (2014a), *MNRAS*, **440**, 1322. Copyright 2014 Oxford University Press.

Observing Cosmic Shear

Systematics

- *PSF corrections*
  color dependance

- *redshifts*
  photometric redshifts are necessary

- *galaxy shape measurement*
  bias estimators

$$\boldsymbol{\epsilon}^{\mathrm{obs}} = (1 + m)\boldsymbol{\epsilon}^{\mathrm{true}} + \mathbf{c}$$

- *Intrinsic alignments & GI correlations*

•PSF corrections

The PSF varies with color so galaxies will have different PSF than the stars and each other.

There are color gradients within galaxies so a purely color dependent correction is not perfect.

Observing Cosmic Shear Systematics

- *PSF corrections*
  color dependance

- *redshifts*
  photometric redshifts are necessary

- *galaxy shape measurement*
  bias estimators

$$\boldsymbol{\epsilon}^{\mathrm{obs}} = (1 + m)\boldsymbol{\epsilon}^{\mathrm{true}} + \mathbf{c} \qquad \begin{array}{l} m \sim 1 - 10\% \\ c \sim 0.1 - 1\% \end{array}$$
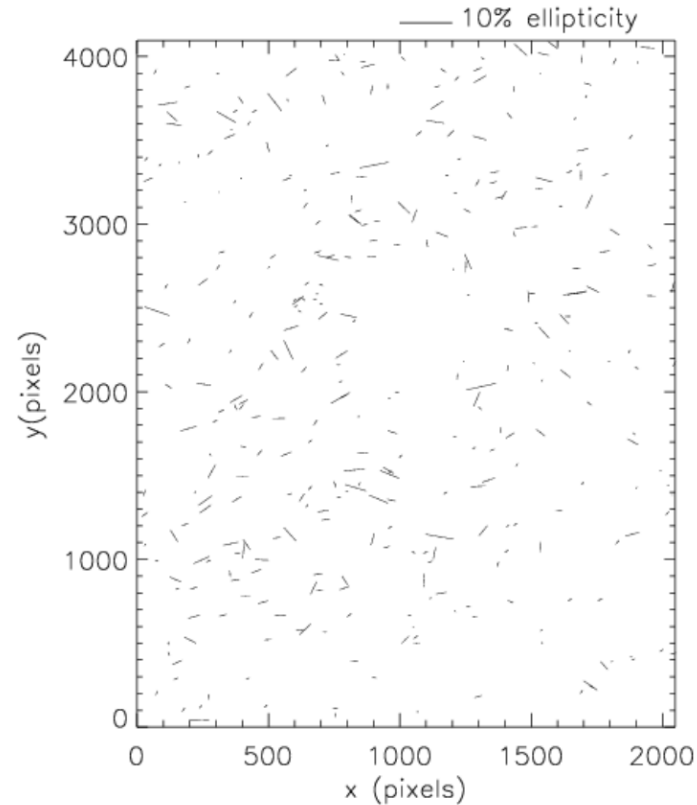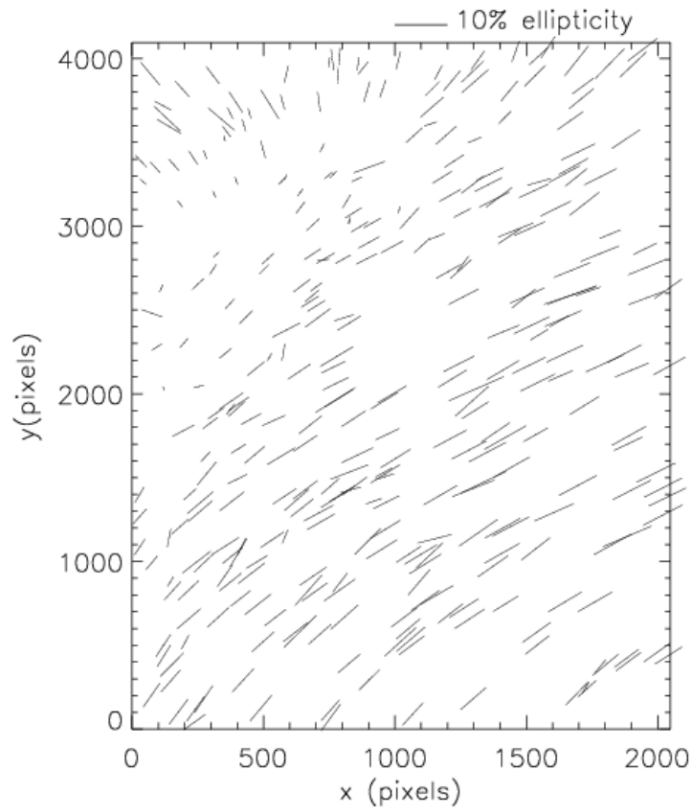
- *Intrinsic alignments & GI correlations*

Observing Cosmic Shear Systematics

Intrinsic alignments & GI term

$$\hat{\xi}_{\pm} = \frac{\sum_{ij} w_i w_j \left[\epsilon_{\parallel}^{(i)} \epsilon_{\parallel}^{(j)} \pm \epsilon_{\wedge}^{(i)} \epsilon_{\wedge}^{(j)} \right]}{\sum_{ij} w_i w_j}$$

$$\vec{\epsilon} \simeq \vec{\gamma} + \vec{\epsilon}_o$$

There are three types of terms in this correlation function

shear-shear

$$\left\langle \gamma^{(i)} \gamma^{(j)} \right\rangle$$

GG correlation

$$\left\langle \epsilon_o^{(i)} \gamma^{(j)} \right\rangle$$

elipticity-elipticity

$$\left\langle \epsilon_o^{(i)} \epsilon_o^{(j)} \right\rangle$$

II correlation

$\epsilon_o^{(i)}$

$\epsilon_o^{(j)}$

Observing Cosmic Shear Systematics

Intrinsic alignments & GI term

$$\hat{\xi}_\pm = \frac{\sum_{ij} w_i w_j \left[\epsilon_\parallel^{(i)} \epsilon_\parallel^{(j)} \pm \epsilon_\wedge^{(i)} \epsilon_\wedge^{(j)} \right]}{\sum_{ij} w_i w_j}$$

$$\vec{\epsilon} \simeq \vec{\gamma} + \vec{\epsilon}_o$$
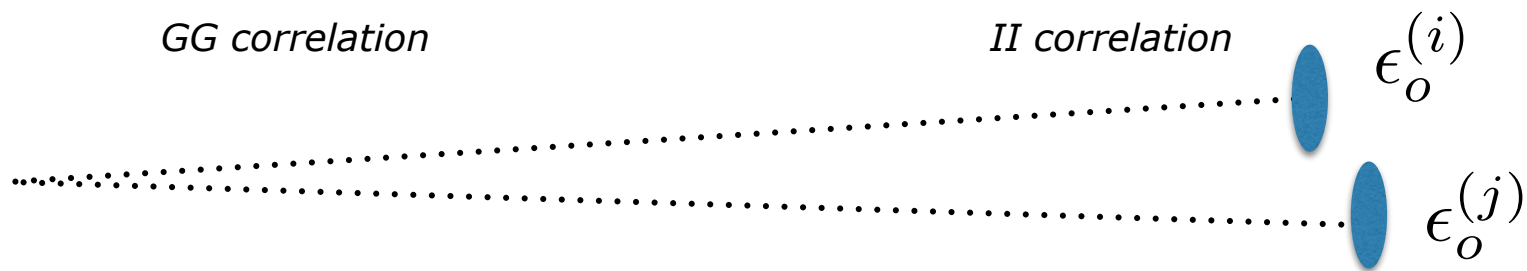
There are three types of terms in this correlation function

shear-shear

$$\langle \gamma^{(i)} \gamma^{(j)} \rangle$$

GG correlation

shear-ellipticity

$$\langle \epsilon_o^{(i)} \gamma^{(j)} \rangle$$

GI correlation

elipticity-elipticity

$$\langle \epsilon_o^{(i)} \epsilon_o^{(j)} \rangle$$

II correlation

$$\epsilon_o^{(i)}$$

$$\gamma^{(j)}$$
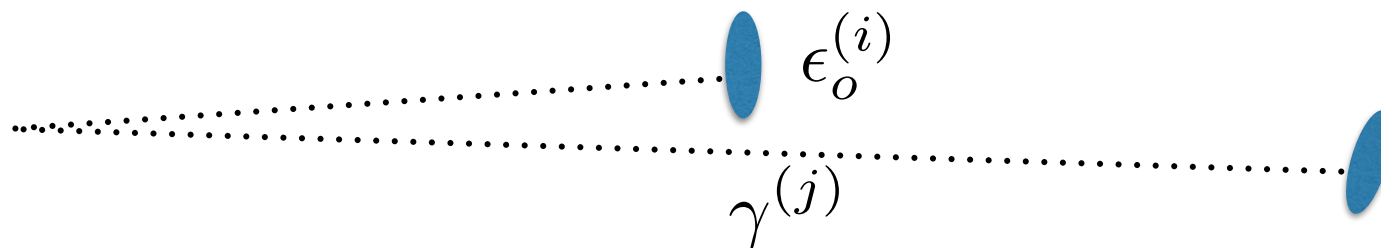
Observations

Weak lensing surveys, to lowest order, measure
a combination of cosmological parameters
given by

matter density

$$S_8 = \sigma_8 \left(\frac{\Omega_m}{0.3} \right)^{\alpha}$$

power spectrum
normalisation

$$\alpha \simeq 0.5$$

Weakly depending on
the redshift
distribution of sources.

from M. Kilbinger 2014

Observations

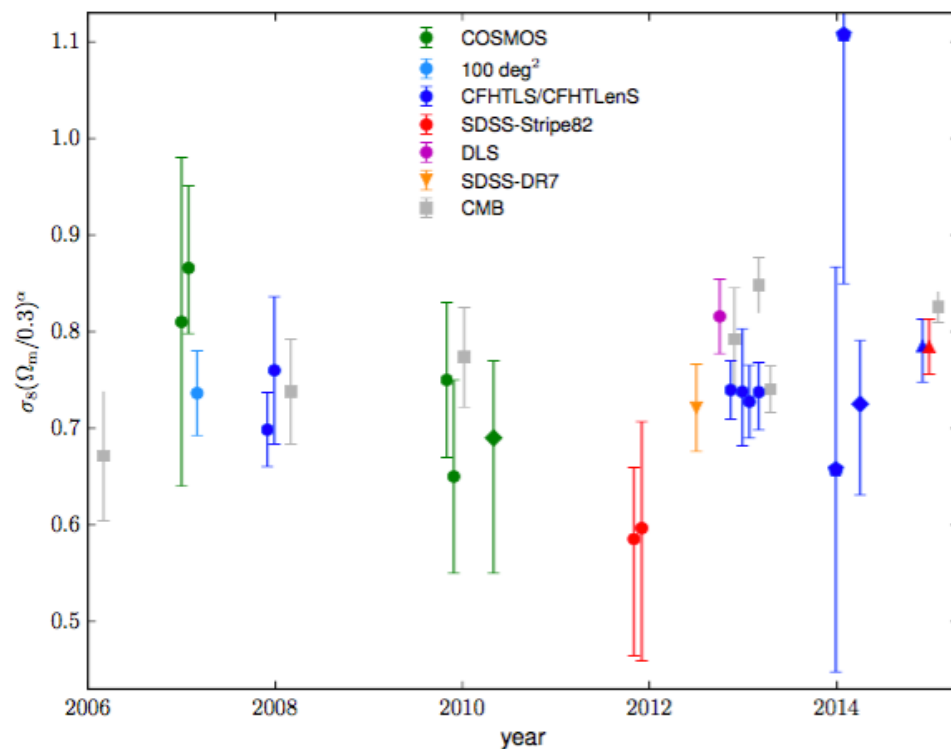| Survey	$\sigma_8(\Omega_{\rm m}/0.3)^\alpha$	original measurement	N_z	Reference
COSMOS	0.81 ± 0.17	$\sigma_8(\Omega_{\rm m}/0.3)^{0.48} = 0.81 \pm 0.17$	1	Massey et al. (2007b)
COSMOS	$0.87^{+0.09}_{-0.07}$	$\sigma_8(\Omega_{\rm m}/0.3)^{0.44} = 0.866^{+0.085}_{-0.068}$	3	Massey et al. (2007b)
100 deg^2	0.74 ± 0.04	$\sigma_8(\Omega_{\rm m}/0.24)^{0.59} = 0.84 \pm 0.05$	1	Benjamin et al. (2007)
CFHTLS	0.70 ± 0.04	$\sigma_8(\Omega_{\rm m}/0.25)^{0.64} = 0.785 \pm 0.043$	1	Fu et al. (2008)
CFHTLS	0.76 ± 0.08	$\sigma_8(\Omega_{\rm m}/0.25)^{0.53} = 0.837 \pm 0.084$	1	Fu et al. (2008), large scales
COSMOS	0.75 ± 0.08	$\sigma_8(\Omega_{\rm m}/0.3)^{0.51} = 0.75 \pm 0.08$	$5+1^a$	Schrabback et al. (2010)
COSMOS	0.65 ± 0.10	$\sigma_8(\Omega_{\rm m}/0.3)^{0.62} = 0.65 \pm 0.1$	1	Schrabback et al. (2010)
COSMOS	$0.69^{+0.08}_{-0.14}$	$\sigma_8(\Omega_{\rm m}/0.3)^{0.46} = 0.69^{+0.08}_{-0.14}$	1	Semboloni et al. (2011b), +IA
SDSS-Stripe82	$0.59^{+0.07}_{-0.12}$	$\sigma_8(\Omega_{\rm m}/1.0)^{0.7} = 0.252^{+0.032}_{-0.052}$	1	Lin et al. (2012)
SDSS-Stripe82	$0.60^{+0.11}_{-0.14}$	$\sigma_8(\Omega_{\rm m}/0.264)^{0.67} = 0.65^{+0.12}_{-0.15}$	1	Huff et al. (2014a)
SDSS-DR7	0.72 ± 0.05	$\sigma_8(\Omega_{\rm m}/0.25)^{0.57} = 0.8 \pm 0.05$	1	Mandelbaum et al. (2013)
DLS	0.82 ± 0.04	$\sigma_8(\Omega_{\rm m}/0.265)^{0.5} = 0.868 \pm 0.041$	1	Jee et al. (2013), priv. comm.
CFHTLenS	0.74 ± 0.03	$\sigma_8(\Omega_{\rm m}/0.27)^{0.59} = 0.787 \pm 0.032$	1	Kilbinger et al. (2013)
CFHTLenS	$0.74^{+0.07}_{-0.06}$	$\sigma_8(\Omega_{\rm m}/0.27)^{0.65} = 0.79^{+0.07}_{-0.06}$	1	Kilbinger et al. (2013), large scales
CFHTLenS	0.73 ± 0.04	$\sigma_8(\Omega_{\rm m}/0.27)^{0.55} = 0.771 \pm 0.04$	2	Benjamin et al. (2013)
CFHTLenS	$0.74^{+0.03}_{-0.04}$	$\sigma_8(\Omega_{\rm m}/0.27)^{0.46} = 0.774^{+0.032}_{-0.041}$	6	Heymans et al. (2013), +IA
CFHTLenS	0.66 ± 0.21	$\sigma_8(\Omega_{\rm m}/0.27)^{0.46} = 0.69 \pm 0.22$	∞^b	Kitching et al. (2014)
CFHTLenS	1.11 ± 0.26	$\sigma_8(\Omega_{\rm m}/0.27)^{0.44} = 1.16 \pm 0.27$	∞^b	Kitching et al. (2014), large scales
CFHTLenS	$0.73^{+0.07}_{-0.09}$	$\sigma_8(\Omega_{\rm m}/0.27)^{0.57} = 0.77^{+0.07}_{-0.1}$	1	Fu et al. (2014), +IA
CFHTLenS	$0.79^{+0.03}_{-0.04}$	$\sigma_8(\Omega_{\rm m}/0.27)^{0.64} = 0.84^{+0.03}_{-0.04}$	1	Liu et al. (2015)
SDSS-Stripe82	0.78 ± 0.03	$\sigma_8(\Omega_{\rm m}/0.27)^{0.42} = 0.82 \pm 0.03$	1	Liu et al. (2014)
WMAP3^c	0.67 ± 0.07	$\sigma_8(\Omega_{\rm m}/0.234)^{0.5} = 0.76 \pm 0.05$	-	Spergel et al. (2007)
WMAP5^c	0.74 ± 0.05	$\sigma_8(\Omega_{\rm m}/0.258)^{0.5} = 0.796 \pm 0.036$	-	Komatsu et al. (2009)
WMAP7^c	0.77 ± 0.05	$\sigma_8(\Omega_{\rm m}/0.273)^{0.5} = 0.811^{+0.03}_{-0.031}$	-	Komatsu et al. (2011)
WMAP9	0.79 ± 0.05	$\sigma_8(\Omega_{\rm m}/1.0)^{0.5} = 0.434 \pm 0.029$	-	Hinshaw et al. (2013)
Planck2013	0.85 ± 0.03	$\sigma_8(\Omega_{\rm m}/0.27)^{0.46} = 0.89 \pm 0.03$	-	Planck Coll. (2014a), $C(\ell)$
Planck2013	0.74 ± 0.02	$\sigma_8(\Omega_{\rm m}/0.27)^{0.3} = 0.764 \pm 0.025$	-	Planck Coll. (2014b), SZ
Planck2015	0.83 ± 0.02	$\sigma_8(\Omega_{\rm m}/1.0)^{0.5} = 0.4521 \pm 0.0088$	-	Planck Coll. (2015), $C(\ell)$

CMB

from M. Kilbinger 2014

Observations
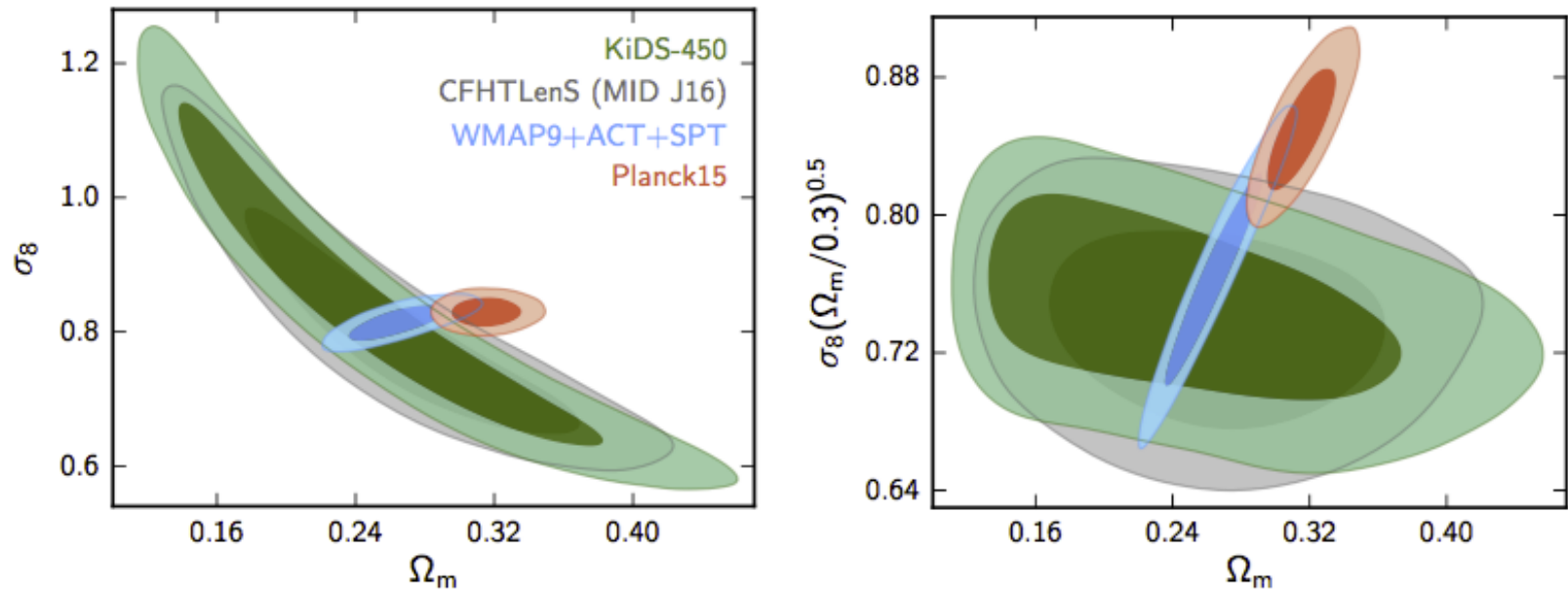
Figure 6. Marginalized posterior contours (inner 68% CL, outer 95% CL) in the Ω_m-σ_8 plane (left) and Ω_m-S_8 plane (right) from the present work (green), CFHTLenS (grey), pre-Planck CMB measurements (blue), and Planck 2015 (orange). Note that the horizontal extent of the confidence contours of the lensing measurements is sensitive to the choice of the prior on the scalar spectrum amplitude A_s. The CFHTLenS results are based on a more informative prior on A_s artificially shortening the contour along the degeneracy direction.

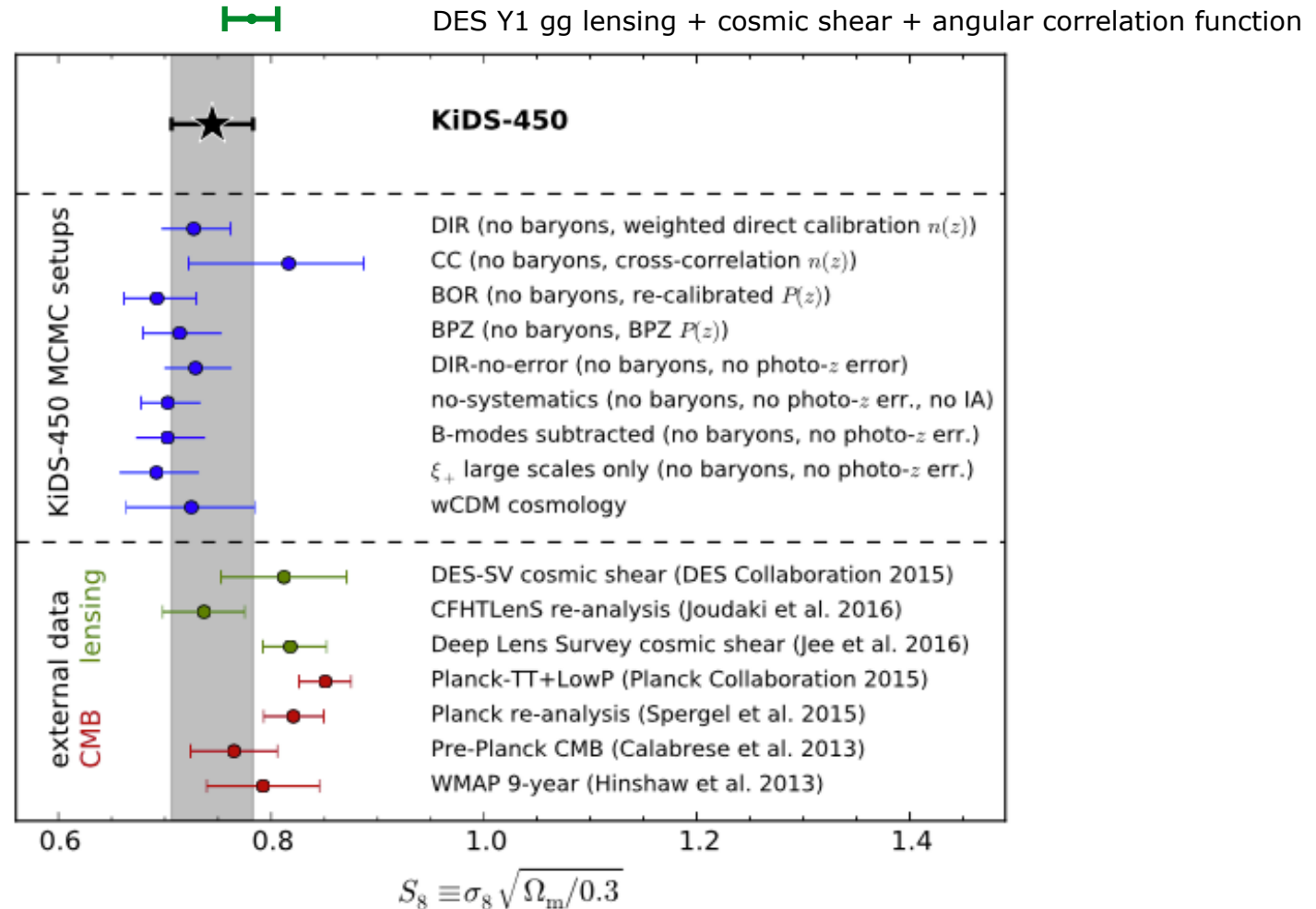*Hildebrandt, et al. 2016*
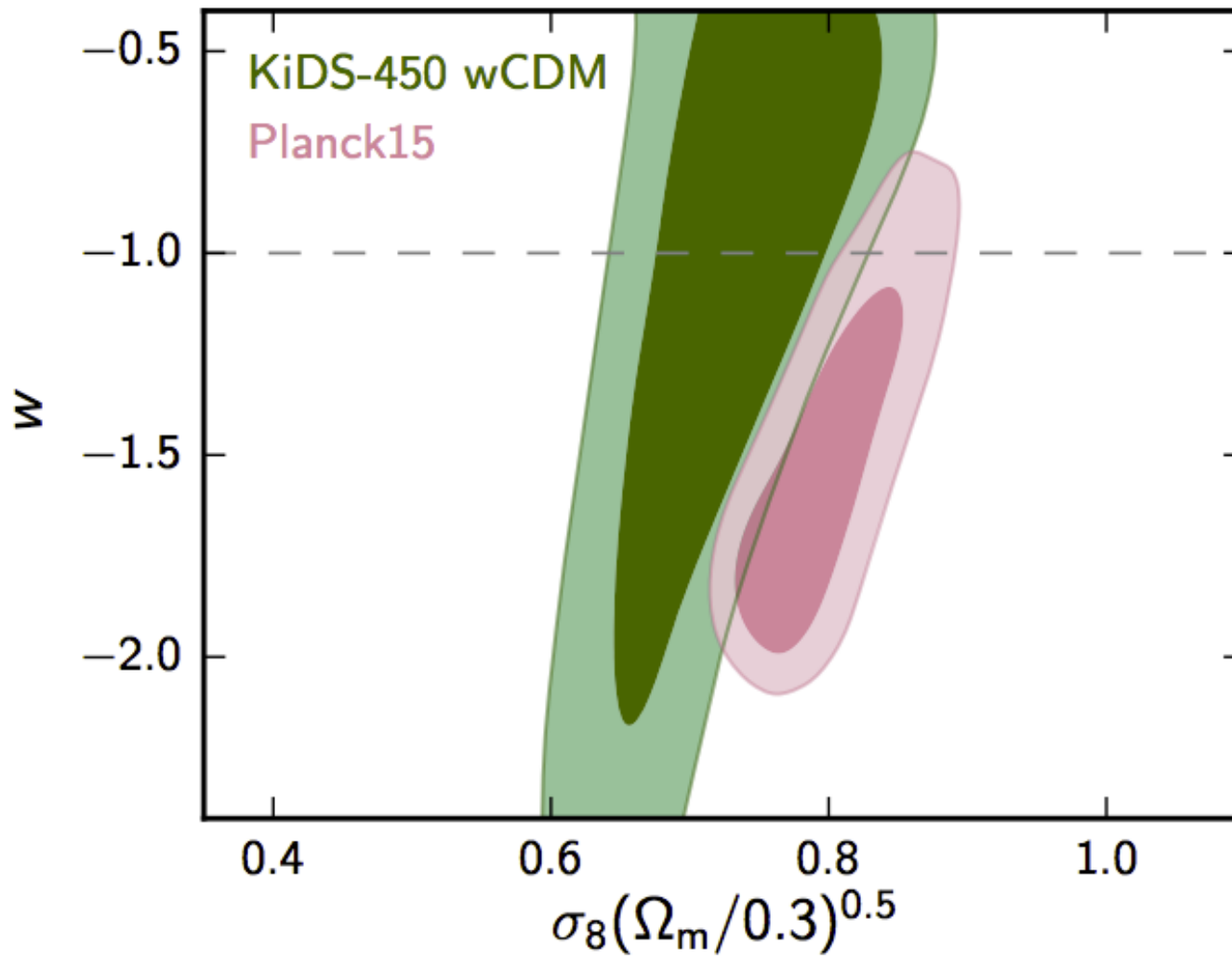
Observations

Figure 9. Marginalized posterior contours (inner 68% CL, outer 95% CL) in the S_8-w plane from KiDS-450 (green) and Planck 2015 (pink).

Hildebrandt, et al. 2016

Observations

Figure 10. Constraints on S_8 for the different runs considered in the KiDS-450 analysis as well as several literature measurements. The grey band indicates the 1σ constraints from our primary analysis. Note that most of the runs which test for systematic errors (blue data points) switch off some of the astrophysical or redshift systematics. Hence not all data points shown here are fully comparable. For numerical values of the plotted data points see Table F1.
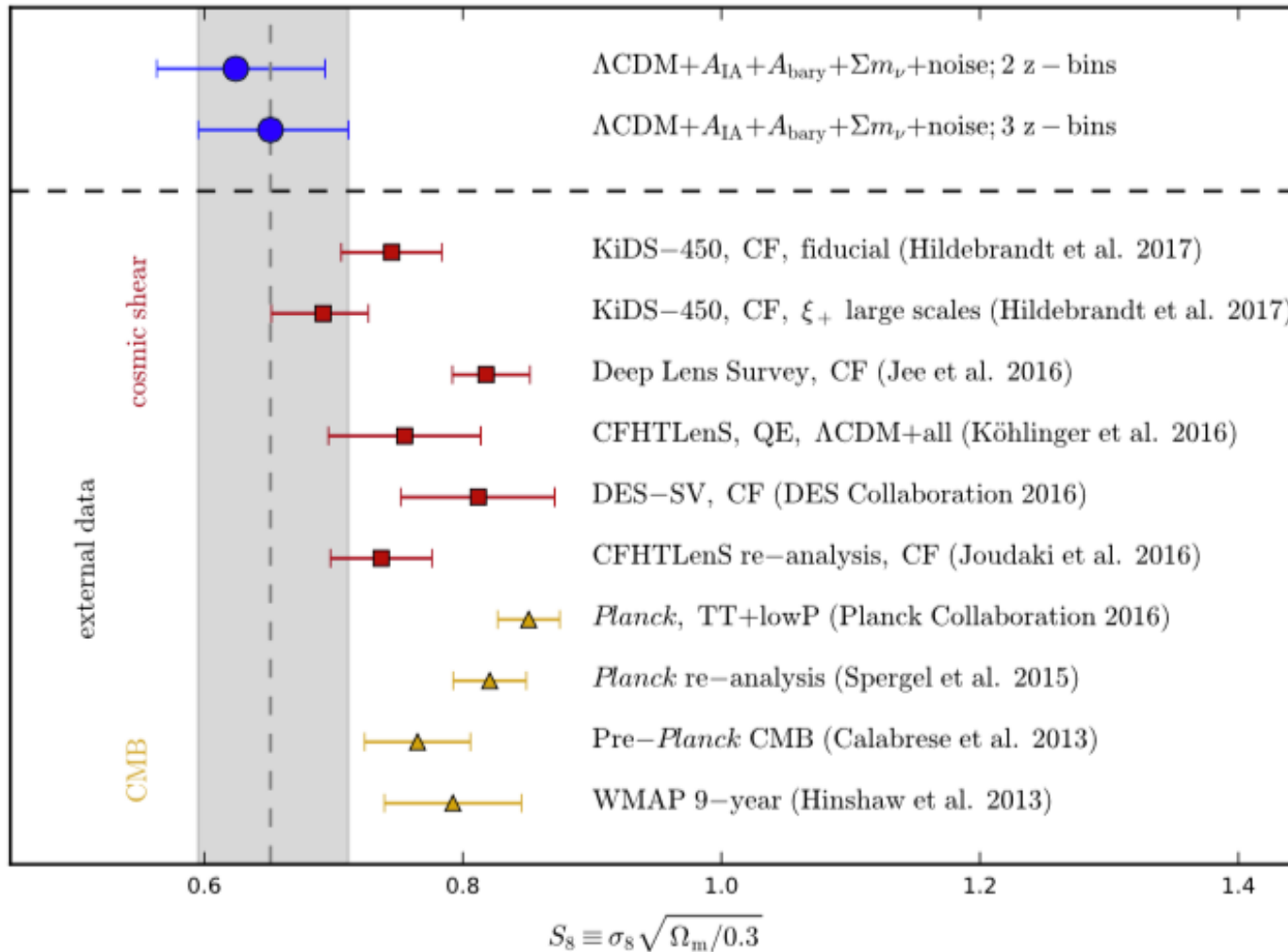
Hildebrandt, et al. 2016

Observations

$$S_8 = 0.783^{+0.021}_{-0.025}$$

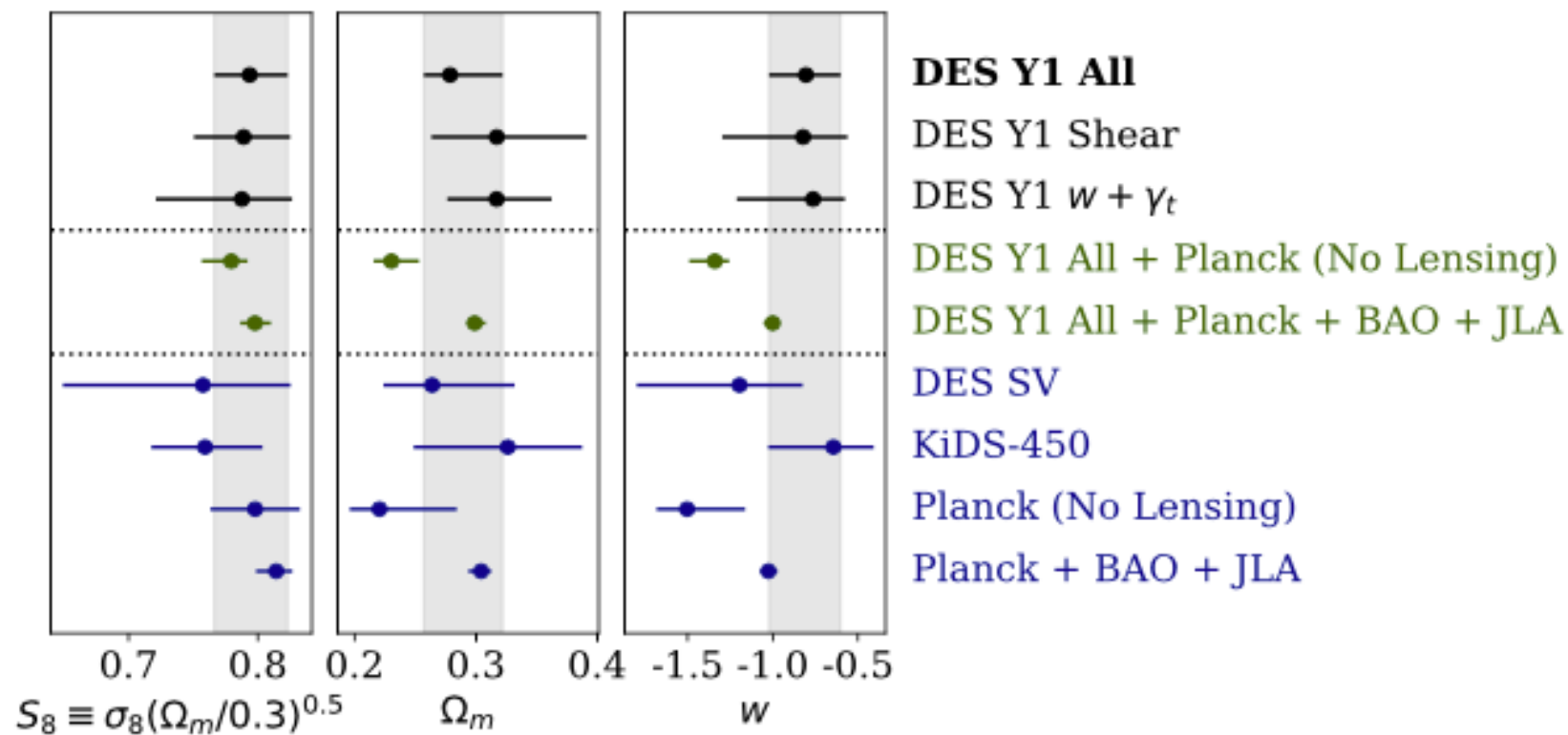DES Y1 gg lensing + cosmic shear + angular correlation function

KiDS-450

$\Lambda\text{CDM}+A_{\text{IA}}+A_{\text{bary}}+\Sigma m_\nu+\text{noise}; 2\,z-\text{bins}$

$\Lambda\text{CDM}+A_{\text{IA}}+A_{\text{bary}}+\Sigma m_\nu+\text{noise}; 3\,z-\text{bins}$

cosmic shear

KiDS$-$450, CF, fiducial (Hildebrandt et al. 2017)

KiDS$-$450, CF, ξ_+ large scales (Hildebrandt et al. 2017)

Deep Lens Survey, CF (Jee et al. 2016)

CFHTLenS, QE, ΛCDM+all (Köhlinger et al. 2016)

DES$-$SV, CF (DES Collaboration 2016)

external data

CFHTLenS re$-$analysis, CF (Joudaki et al. 2016)

Planck, TT+lowP (Planck Collaboration 2016)

Planck re$-$analysis (Spergel et al. 2015)

Pre$-$*Planck* CMB (Calabrese et al. 2013)

CMB

WMAP 9$-$year (Hinshaw et al. 2013)

0.6   0.8   1.0   1.2   1.4

$$S_8 \equiv \sigma_8 \sqrt{\Omega_{\text{m}}/0.3}$$

Köhlinger, et al. 2017

Observations

DES Y1

DES Y1 All
DES Y1 Shear
DES Y1 $w + \gamma_t$
DES Y1 All + Planck (No Lensing)
DES Y1 All + Planck + BAO + JLA
DES SV
KiDS-450
Planck (No Lensing)
Planck + BAO + JLA

$S_8 \equiv \sigma_8 (\Omega_m / 0.3)^{0.5}$ Ω_m w

Abbott, et al. 2017

Observations

Future :
- more from KiDS
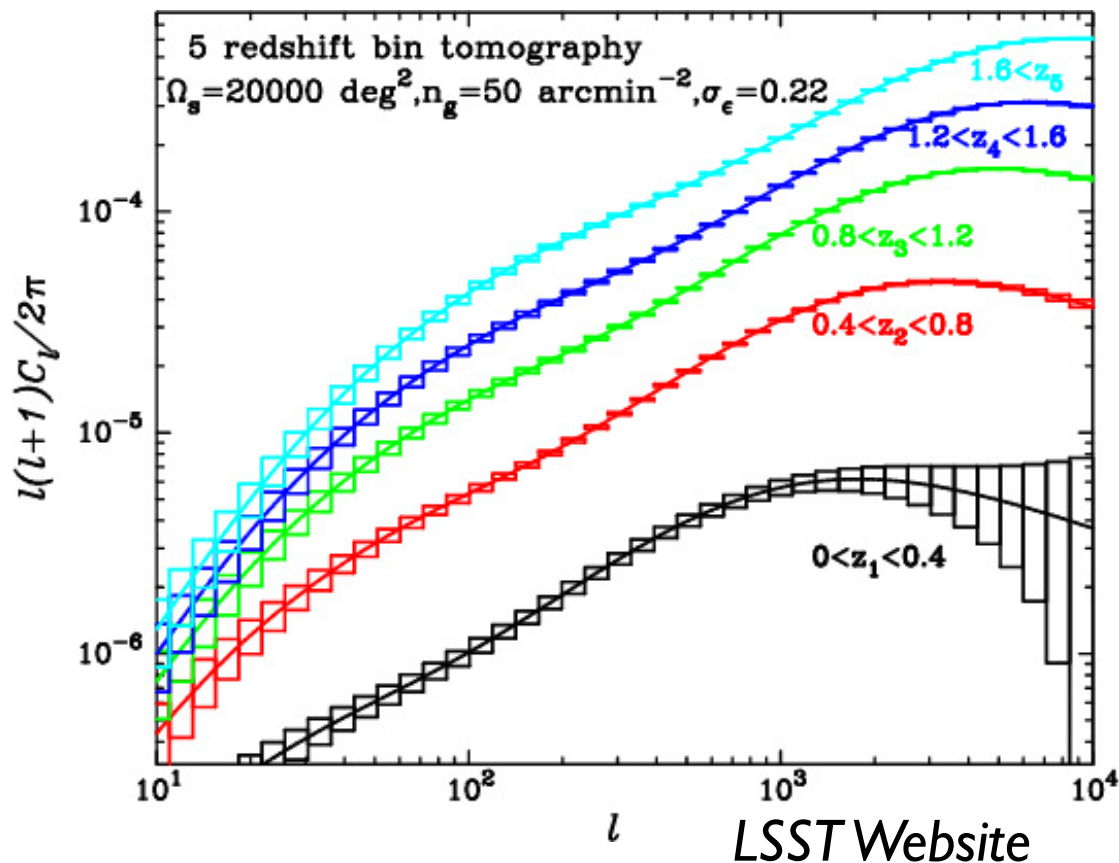- more from Dark Energy Survey (DES)
- Hyper SuprimeCam (HSC)
- Large Synoptic Survey Telescope (LSST)
- Wide Field Infrared Survey Tel. (WFIRST)
- Euclid

Convergence Power Spectra for multiple source redshift bins

5 redshift bin tomography
$\Omega_s = 20000 \ deg^2, n_g = 50 \ arcmin^{-2}, \sigma_\epsilon = 0.22$

$1.6 < z_5$
$1.2 < z_4 < 1.6$
$0.8 < z_3 < 1.2$
$0.4 < z_2 < 0.8$
$0 < z_1 < 0.4$
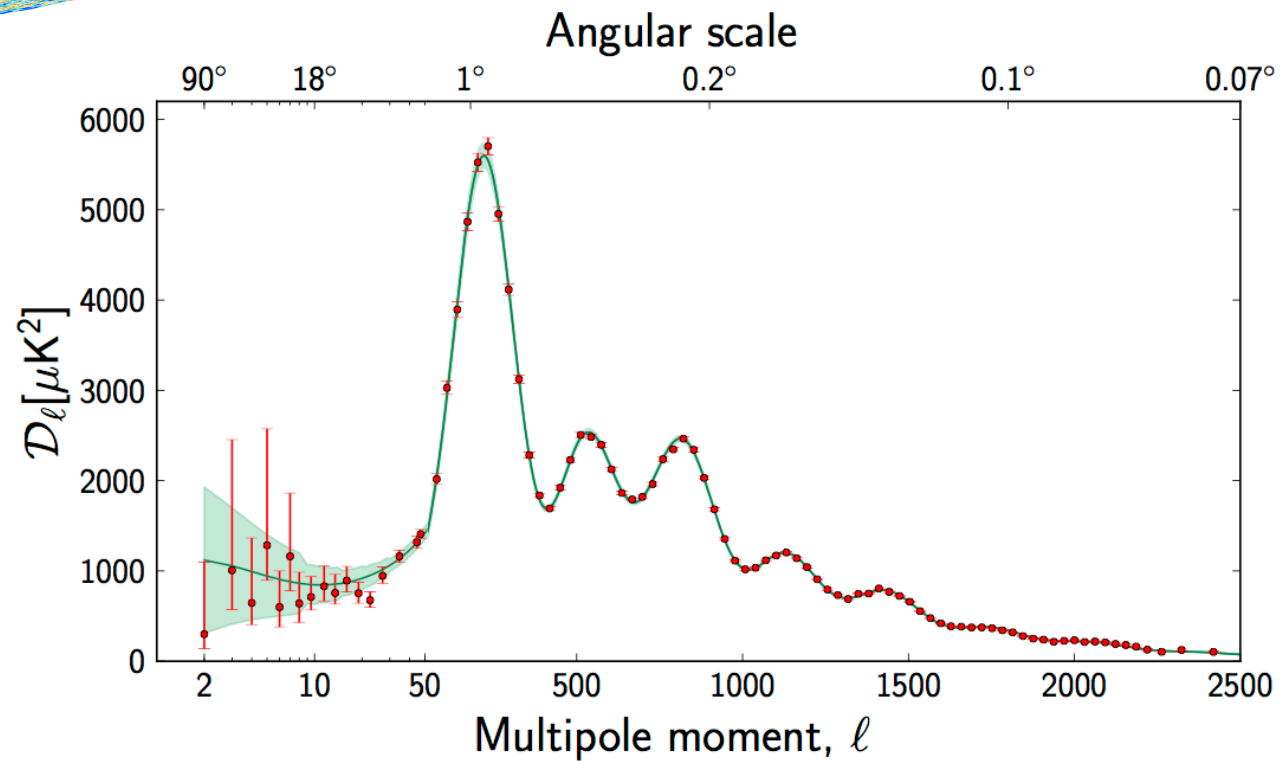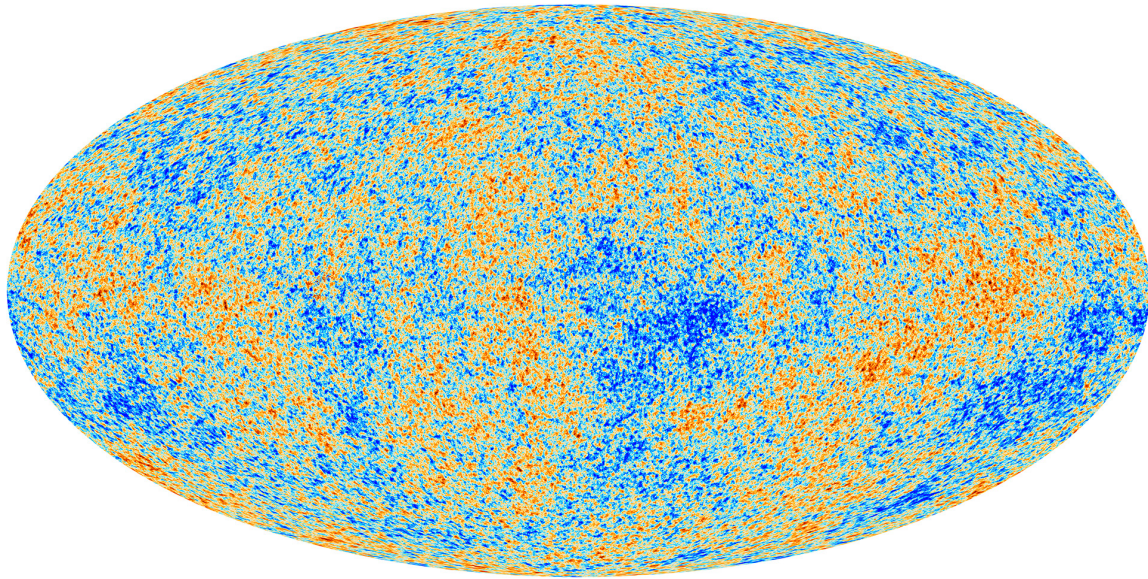
y-axis: $l(l+1)C_\nu/2\pi$
x-axis: l

LSST Website

With redshift information, and enough galaxies, the shear power spectrum can measured as a function of source redshift.

The redshifts for so many galaxies need to be measured by photometric redshifts.

This will probe the evolution in the energy densities of the universe as a function of redshift.

Lensing of the CMB

Planck Observations

CMB Power Spectrum

Lensing will make the local power spectrum anisotropic and magnified.

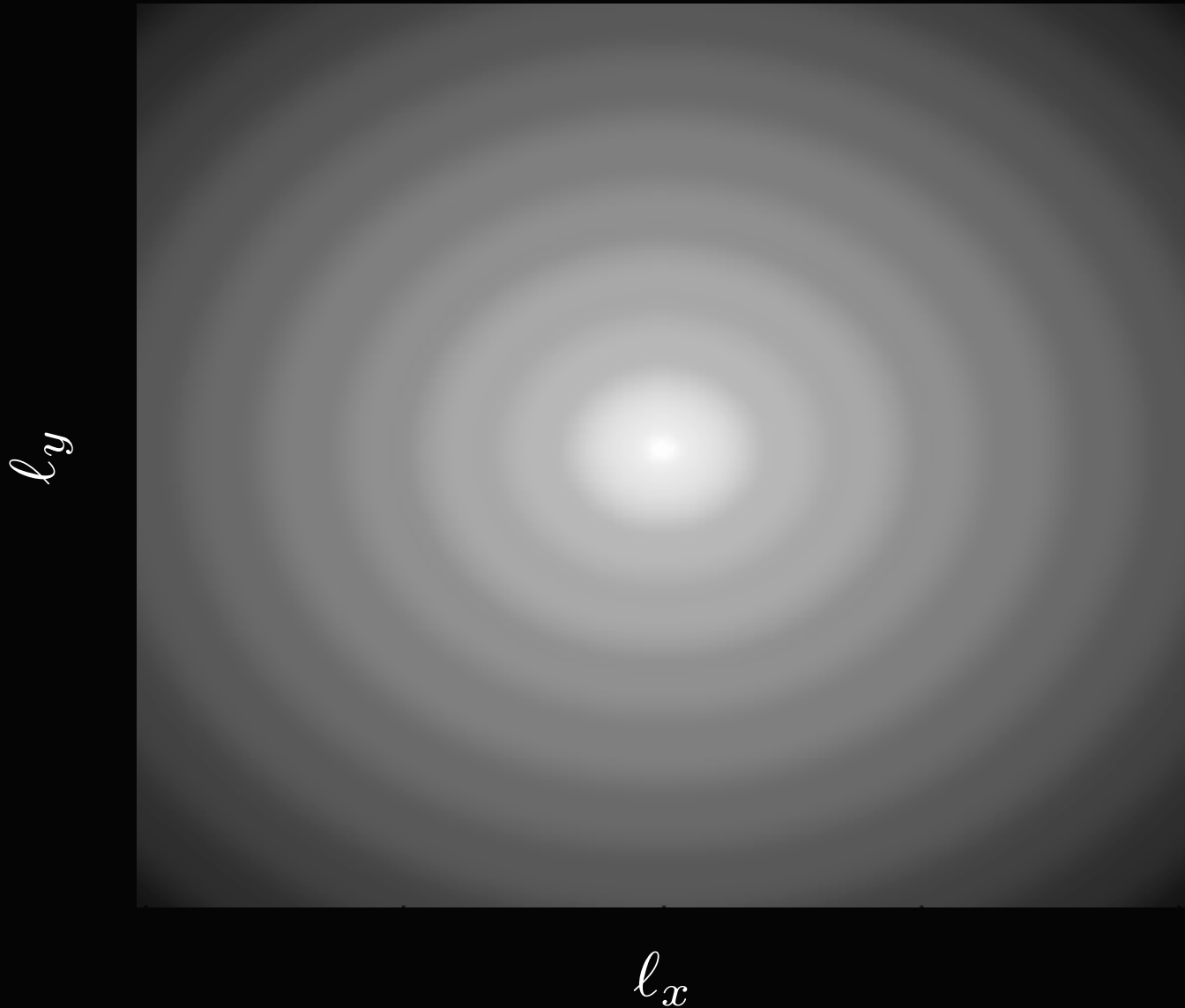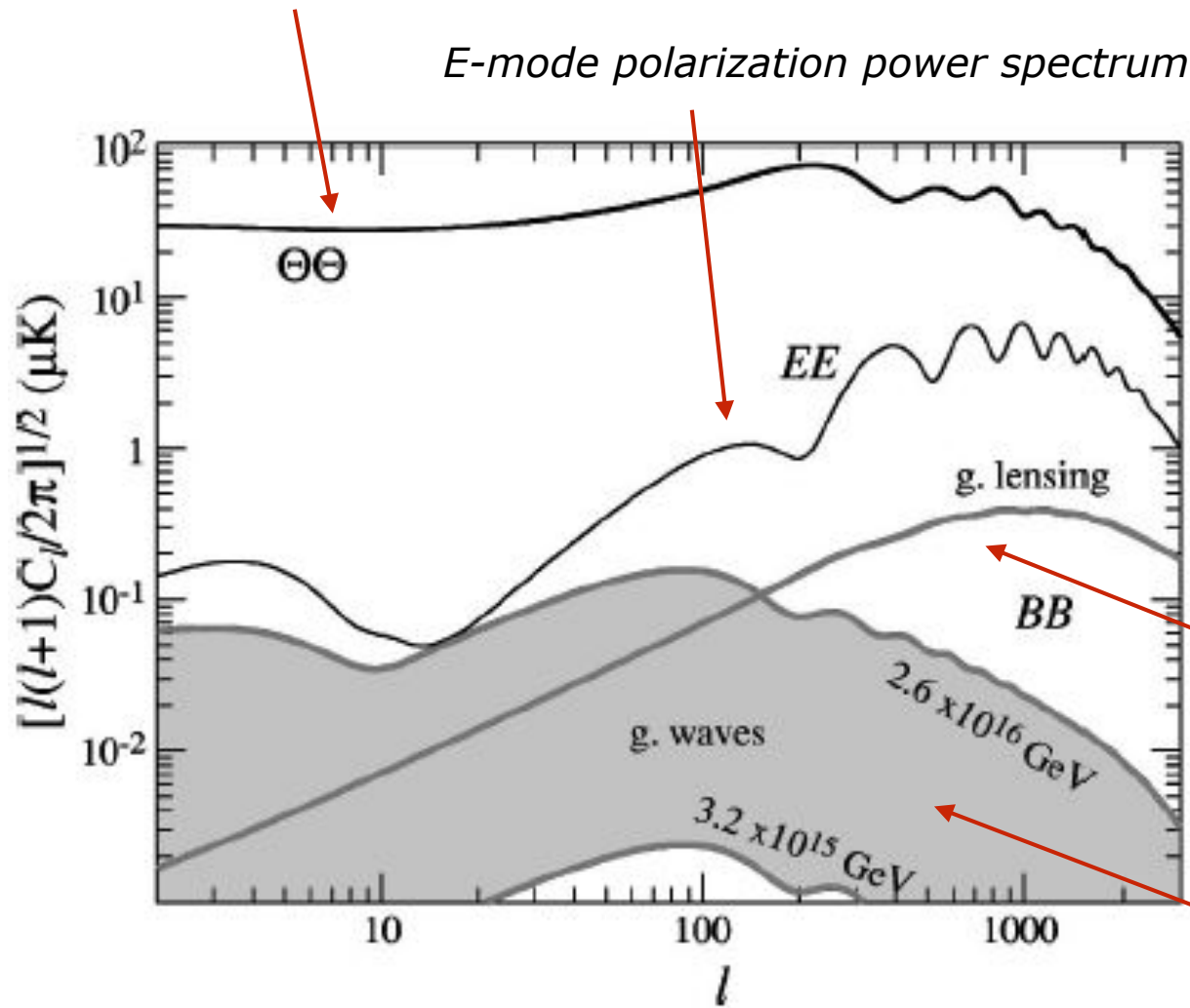# CMB Power Spectrum

Lensing will make the local power spectrum anisotropic and magnified.

Lensing of the CMB

Temperature power spectrum

E-mode polarization power spectrum

Primordial B-mode polarization cannot be produced by scalar perturbations.

They are produced by primordial gravity waves.

And by gravitational lensing.

Lensing induced B-mode polarization power spectrum

Range of primordial B-mode polarization power spectrum

$$\tilde{C}_l^X = C_l^X + \int \frac{d^2 l'}{(2\pi)^2} \left[l' \cdot (1 - l') \right]^2 e^{2i(\phi_{l'} - \phi_l)} C_{|1-l'|}^\psi C_{|l'|}^X - C_l^X \int \frac{d^2 l'}{(2\pi)^2} (l' \cdot 1)^2 C_{l'}^\psi. \qquad X = E, B$$
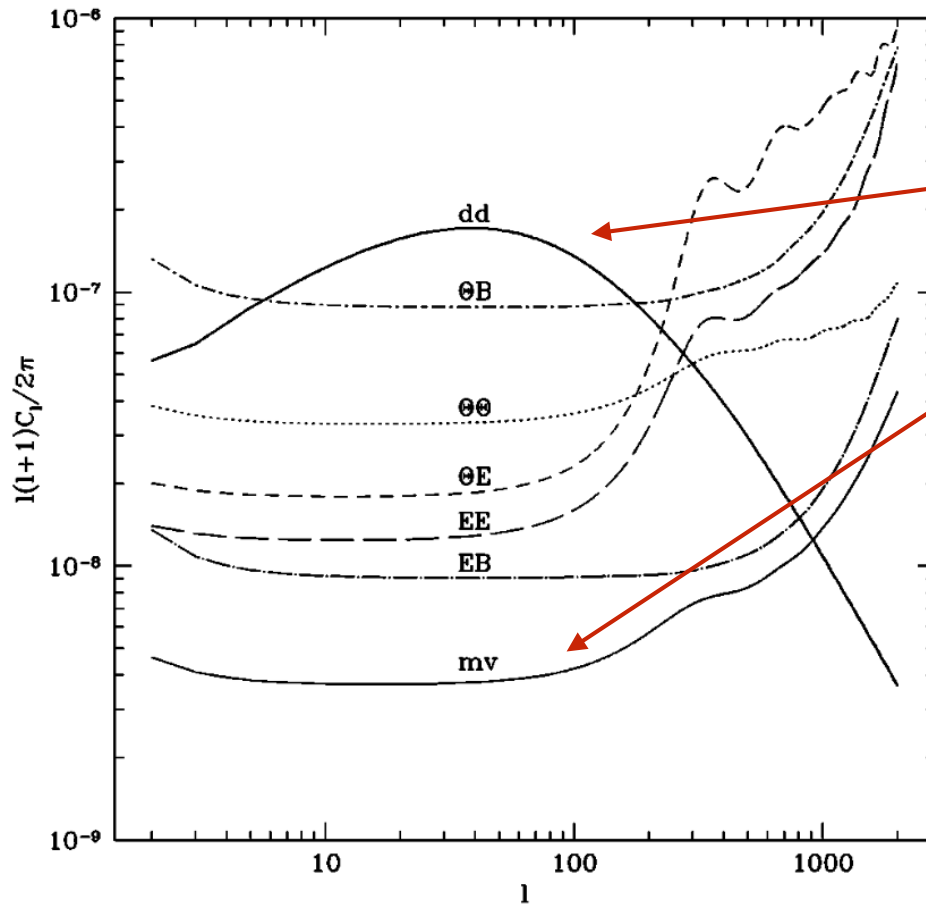
Lensing of the CMB

FIG. 1. Deflection and noise power spectra for the quadratic and minimum variance estimators, assuming the noise properties of the reference experiment ($\Delta_\Theta=1$ μK arcmin; $\Delta_P=\sqrt{2}$ μK arcmin; $\theta_{\mathrm{FWHM}}=4'$) and a fiducial ΛCDM cosmology with parameters $\Omega_c=0.3$, $\Omega_b=0.05$, $\Omega_\Lambda=0.65$, $h=0.65$, $n=1$, $\delta_H=4.2\times10^{-5}$ and no gravitational waves.

Deflection power spectrum
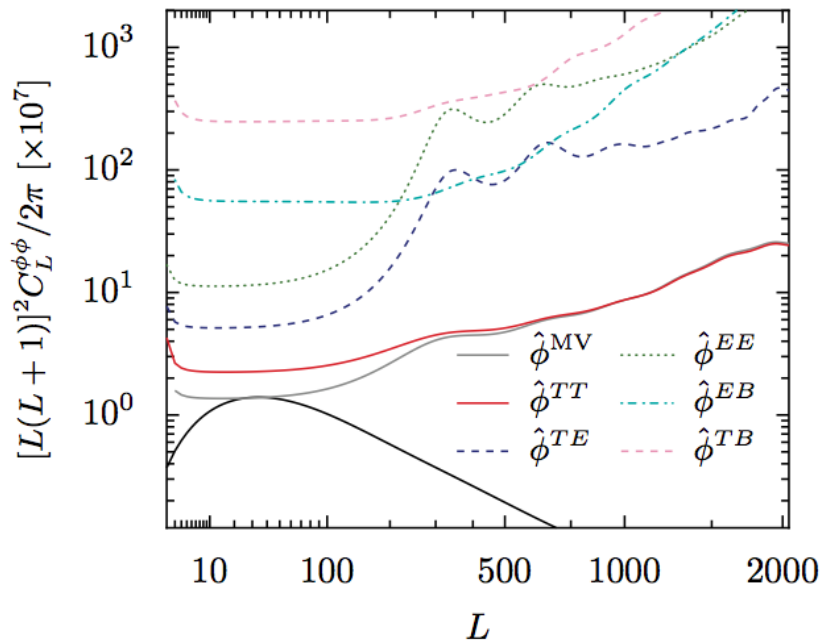
Total noise in deflection reconstruction

Primordial B-mode polarization cannot be produced by scalar perturbations.

They are produced by primordial gravity waves.

And by gravitational lensing.

Okamato & Hu 2003

$$\tilde{C}_l^X = C_l^X + \int \frac{d^2 l'}{(2\pi)^2} \, [l' \cdot (l-l')]^2 \, e^{2i(\phi_{l'}-\phi_l)} C_{|l-l'|}^\psi C_{|l'|}^X - C_l^X \int \frac{d^2 l'}{(2\pi)^2} (l' \cdot l)^2 C_{l'}^\psi. \qquad X = E, B$$

Lensing of the CMB

Planck Observations

Noise Levels

map of the lensing potential

Fig. 1. Lens reconstruction noise levels $N_L^{\phi\phi}$ for the TT, TE, EE, EB, and TB estimators applied to the SMICA full-mission CMB map. The noise level for their minimum-variance combination (MV) is also shown. The fiducial ΛCDM theory power spectrum $C_L^{\phi\phi,\text{fid}}$ used in our Monte Carlo simulations is plotted as the black solid line.
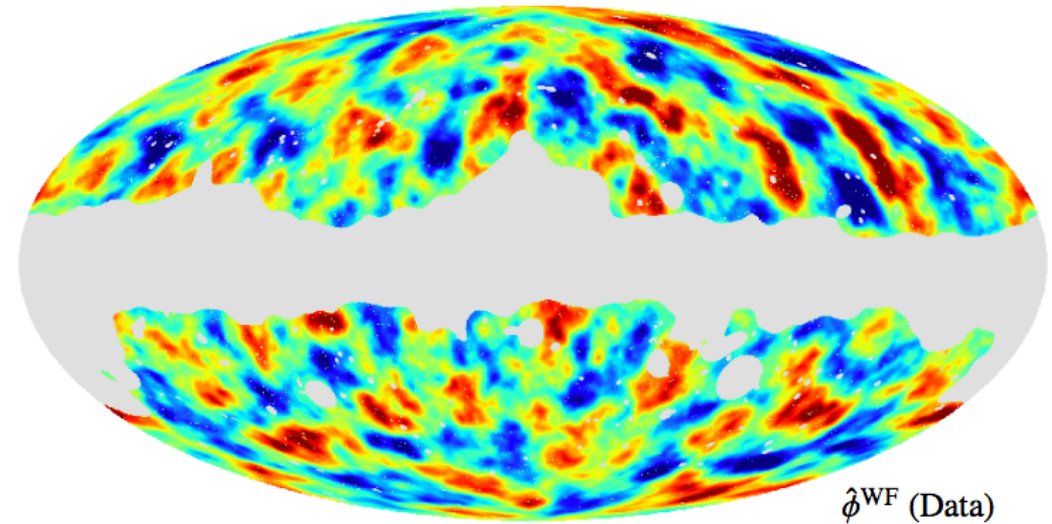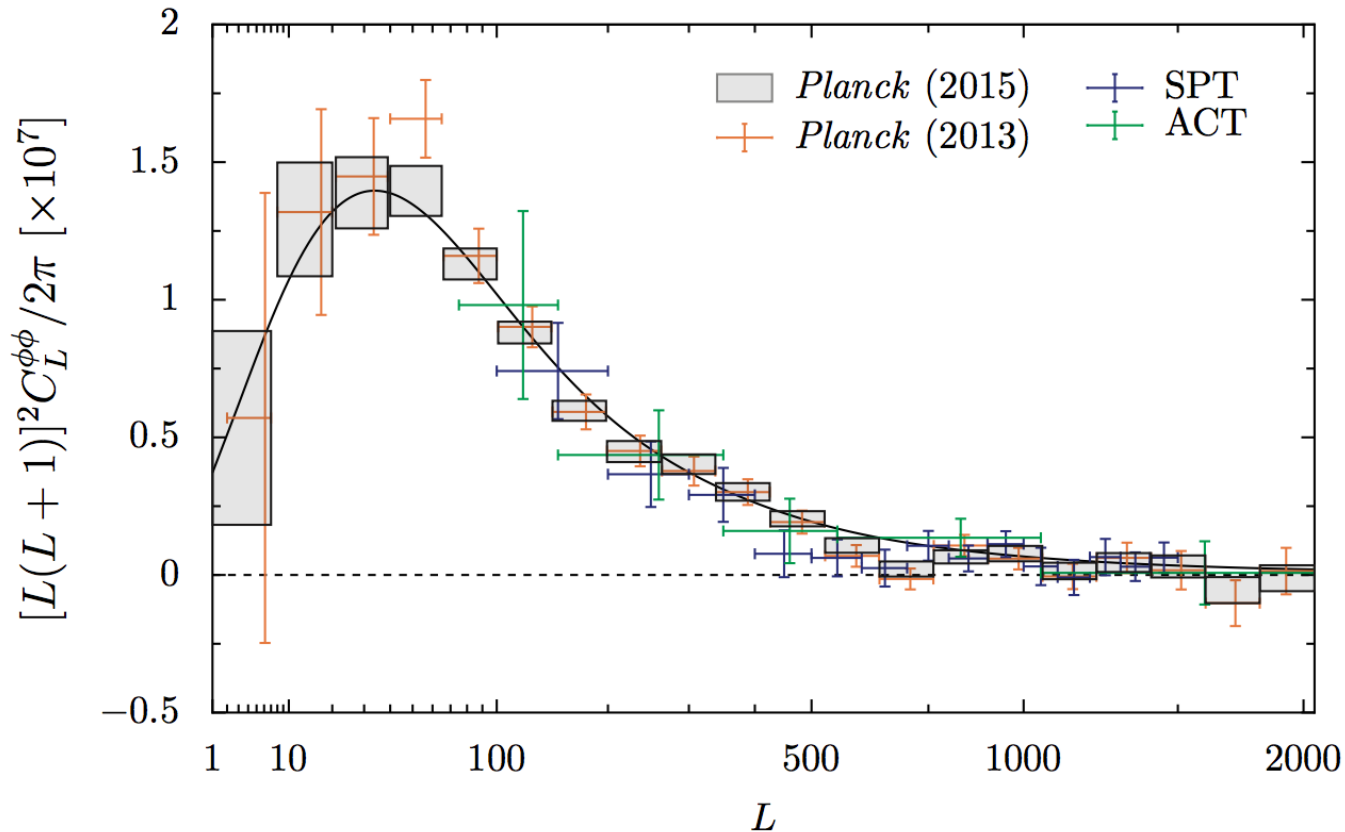
Fig. 2. Lensing potential estimated from the SMICA full-mission CMB maps using the MV estimator. The power spectrum of this map forms the basis of our lensing likelihood. The estimate has been Wiener filtered following Eq. (5), and band-limited to $8 \leq L \leq 2048$.

Abe, et al. 2016, A&A, 594. A15

Planck Satellite Observations

$$S_8 = \sigma_8 \left(\frac{\Omega_m}{0.3}\right)^{0.25} = 0.799 \pm 0.028$$

Fig. 6. *Planck* 2015 full-mission MV lensing potential power spectrum measurement, as well as earlier measurements using the *Planck* 2013 nominal-mission temperature data (Planck Collaboration XVII 2014), the South Pole Telescope (SPT, van Engelen et al. 2012), and the Atacama Cosmology Telescope (ACT, Das et al. 2014). The fiducial ΛCDM theory power spectrum based on the parameters given in Sect. 2 is plotted as the black solid line.

Abe, et al. 2016, A&A, 594. A15

Other topics in gravitational lensing & cosmology

- Density reconstruction in galaxy clusters using weak lensing

- Strong lensing reconstruction of galaxies, groups and cluster

- Strong lensing time-delays as a measure of the Hubble constant

- Probing small scale structure with strong lensing

- Using lenses as gravitational telescopes to survey high redshifts

- Weak lensing from high redshift 21 cm radiation

- Weak lensing from the Lyman alpha forest

References (to get started):

Gravitational Lensing
  Schneider, Ehlers. & Falco (1992), Springer
    text book
Galaxy-Galaxy lensing
  Mandelbaum, et al. 2006, MNRAS, 368, 715
    SDSS results
  Clampitt, 2016, arXiv:1603.05790
    DES results
Weak lensing
  Kilbinger, (2014) arXiv:1411.0115
    review of weak lensing
  Bartelman & Schneider (2001) Phys.Rep. 340, 291
    review of weak lensing
  Hildebrandt, et al. (2017), arXiv:1606.05338
    KiDS-450 results
  Köhlinger, et al. (2017), arXiv:1706.02892
    KiDS-450 results
  Giocoli, et al. (2016), MNRAS, 461, 209
    simulating gravitational lensing
  Tessore, et al. (2015), JCAP, 10, 036
    simulations with some alternative gravity theories
CMB Lensing
  Lewis & Challinor, 2006, Phys.Rept. 429, 1, arXiv:astro-ph/0601594
    review of theory
  "Planck 2015 results - XV. Gravitational lensing", 2016,A&A,594,A15
    observations